How Well Do Empirical Molecular Mechanics Force Fields Model the Cholesterol Condensing Effect?

J. Sawdon,[1] T. J. Piggot,[2,1,a)] and J. W. Essex[1,b)]
[1)] *School of Chemistry, University of Southampton, Highfield, Southampton, SO17 1BJ, UK*
[2)] *Chemical, Biological and Radiological Sciences Division, Defense Science and Technology Laboratory (DSTL), Porton Down, Salisbury, Wiltshire, SP4 0JQ, UK*

(Dated: 20 December 2024)

Membrane properties are determined in part by lipid composition, and cholesterol plays a large role in determining these properties. Cellular membranes show a diverse range of cholesterol compositions, the effects of which include alterations to: cellular biomechanics, lipid raft formation, membrane fusion, signalling pathways, metabolism, pharmaceutical therapeutic efficacy, and disease onset. Additionally, cholesterol plays an important role in non-cellular membranes, with its concentration in the skin lipid matrix being implicated in several skin diseases. In phospholipid membranes, cholesterol increases tail ordering of neighboring lipids, decreasing membrane lateral area and increasing thickness. This reduction in lateral area, known as the cholesterol condensing effect, results from cholesterol-lipid mixtures deviating from ideal mixing. Capturing the cholesterol condensing effect is crucial for molecular dynamics simulations as it directly affects the accuracy of predicted membrane properties, which are essential for understanding membrane function. We present a comparative analysis of cholesterol models across several popular force fields: CHARMM36, Slipids, Lipid17, GROMOS 53A6$_L$, GROMOS-CKP, MARTINI 2, MARTINI 3, and ELBA. Simulations of DMPC and DOPC membranes with varying cholesterol concentrations were conducted to calculate partial-molecular areas of cholesterol and other condensing parameters, which are compared to experimental data for validation. While all tested force fields predict small negative deviations from ideal mixing in cholesterol-DOPC membranes, only all-atom force fields capture the larger deviations expected in DMPC membranes. United-atom and coarse-grained models under-predict this effect, condensing fewer neighboring lipids by smaller magnitudes, resulting in too small deviations from ideal mixing. These results suggest that all-atom force fields, particularly CHARMM36 or Slipids, should be used for accurate simulations of cholesterol-containing membranes.

I. INTRODUCTION

Lipid membranes are one of the most widespread cellular structures. While lipid membranes have long been understood to perform as selective barriers that surround cells, an array of additional roles and functions of these membranes has been discovered. For example, membranes can act as regulators of protein function, as a way to segregate intra-cellular components, and as signalling platforms[1,2]. Different membranes, both within and across species, have evolved to perform specific functions determined by the composition and arrangement of their components. For example, animal plasma membranes have evolved to contain a wide-variety of lipids that include many different types of phospholipids, sphingolipids, and sterols. Different lipid species are commonly distributed unevenly, both between membrane leaflets and laterally within a leaflet[3–5]. This differential distribution enables correct membrane function, for example; phosphoinositol lipids, minor components of the plasma membrane, are predominantly located within the cytoplasmic leaflet of the membrane to perform their role in intra-cellular signalling[5].

Within the aforementioned plasma membrane, another lipid component essential for correct membrane function is the sterol molecule cholesterol. Indeed, it is hard to overstate the importance of cholesterol's role as a lipid, as highlighted by its ubiquity in all animal plasma membranes as well as its common occurrence in many other types of membranes. For example, cholesterol has an important role within the stratum corneum membrane and the barrier function of the skin[6]. Cholesterol, makes up a large component of many of the membranes in which it is found; for the example of plasma membranes this is roughly 40 % of the overall lipid content[7]. Much research into the effects of cholesterol on membrane properties over the past century has demonstrated that cholesterol increases ordering of lipid tails and therefore decreases the lateral membrane area while increasing membrane thickness. This increased ordering is believed to arise from the unique structure of cholesterol (Fig 1) which allows it to enhance the packing together of the surrounding membrane lipid tails. The extent of the cholesterol-induced change has been shown to be dependent on the types of lipids comprising the membrane, with greater effects arising with increased lipid tail length and saturation[8–11]. While not the only important physiological function of cholesterol[12], cholesterol specific ordering of lipid tails decreases membrane permeability and fluidity, alters the mechanical properties of the membrane, and is believed to be essential for correct mem-

[a)] t.piggot@soton.ac.uk; tjpiggot@dstl.gov.uk
[b)] j.w.essex@soton.ac.uk

brane lateral heterogeneity[13].

An important property of cholesterol induced lipid ordering is that the reduction observed in membrane area due to cholesterol ordering is not linear with respect to increasing cholesterol concentration. This phenomenon was first reported by Leathes[14] as a tendency for the lateral area of cholesterol containing monolayers to negatively deviate from ideal mixing behaviour. This negative deviation from ideal mixing in cholesterol-lipid membranes has since been termed the cholesterol condensing effect, and is well studied in phosphotidylcholine (PC) lipid membranes both experimentally[9,10,15,16], and computationally[17–27]. Such non-ideal mixing behaviour occurs because at low cholesterol concentrations, each cholesterol molecule is able to impose an ordering effect on multiple neighbouring lipids, causing a decrease in the lateral area of these lipids and therefore a greater overall decrease in membrane area than expected. At higher concentrations, cholesterol molecules are more likely to be closer together, resulting in an overlap of the effective condensing area of each cholesterol molecule, in turn reducing the magnitude of the condensing effect per cholesterol molecule. More recently, Edholm and Nagle have reported that cholesterol has a negative partial-molecular area at low concentrations in simulations of 1,2-dipalmitoyl-sn-glycero-3-phosphocholine (DPPC) bilayers[8], and experimental studies have reported a negative partial-molecular area of cholesterol in 1,2-dimyristoyl-sn-glycero-3-phosphocholine (DMPC) and DPPC membranes[9–11] but a positive value for 1,2-dioleoyl-sn-glycero-3-phosphocholine (DOPC) membranes[11]. Negative partial-molecular areas of cholesterol, where the addition of extra cholesterol molecules results in a smaller overall membrane area, is at the extreme of such non-ideal mixing behaviour and the condensing ability of cholesterol. The differences observed between lipids with two fully saturated (DMPC and DPPC) and two monounsaturated (DOPC) lipid tails, including a lack of observed negative partial-molecular area of cholesterol with DOPC, seemingly arises from a weaker cholesterol condensing ability when combined with more disordered, unsaturated, lipid tails.

Molecular dynamics simulation is a powerful tool for membrane analysis, having been routinely used along-side experimental data to provide molecular level insight into cholesterol containing membrane systems[17,18,23,25–35]. The accuracy of simulations hinges significantly on the ability of force field parameter sets to replicate molecular behaviours. This accuracy is paramount in capturing interactions between system components. Specifically, in cholesterol containing membranes, accurately modelling cholesterol-lipid interactions is essential to correctly model the behaviour of cholesterol. However, until recently, very little work has been published examining cholesterol simulation models[36]. Currently there are several force fields available which may be used to model cholesterol containing membranes but there is a general lack of information regarding the suitability and accuracy of such force field parameters. Recently, the NMRLipids project aimed to address this problem through primarily a comparison of simulations containing varying concentrations of PC lipids and cholesterol to experimental data regarding C-H order parameters, lipid diffusion, and X-ray scattering data[36]. This work demonstrated that all of the force field parameters tested had room for improvement with regards to reproducing these experimental data.

Within this work we sought to further expand the testing of cholesterol force field parameters. In particular, if a force field is to accurately model cholesterol containing membranes, we believe that accurately reproducing the cholesterol condensing effect and predicting partial-molecular areas of cholesterol similar to experimental values, is essential. The following work, therefore, presents a comprehensive comparison of several force fields and cholesterol models for simulating cholesterol in DMPC and DOPC membranes with the goal of examining the ability of force fields to match the experimental condensation data. Additionally, the cholesterol condensing effect in 1-palmitoyl-2-oleoyl-sn-glycero-3-phosphocholine (POPC) membranes is also investigated. The force fields studied are divided into three categories: all-atom force fields (AA), united-atom (UA) force fields, and coarse-grained (CG) force fields. This work, therefore, covers many of the commonly used MD cholesterol force field parameters currently available.

II. MATERIALS AND METHODS

A. Simulation Parameters

Force fields included in this analysis are as follows; i) all-atom force fields: CHARMM36[37], Slipids[38], and Lipid17[39–41], ii) united-atom force fields: GROMOS 53A6$_L$[42] (also called GROMOS 54A7), and GROMOS-CKP[43], and iii) coarse-grained force fields: the MARTINI 2 coarse-grained force field alongside three unique MARTINI cholesterol models, an older model (MARTINI 2.0 cholesterol)[44], the standard cholesterol model used by MARTINI 2 (MARTINI 2.2 cholesterol)[45], and a model by Daily *et al.* (MARTINI Daily *et al.*)[21], the MARTINI 3 force field[46,47], and ELBA, a dual-resolution coarse-grained/ all-atom force field[48]. Cholesterol parameters for both of the GROMOS force fields were taken from a manual entry in the Automated Topology Builder (ATB) database[49,50]. For GROMOS-CKP, parameters published by Bachar *et al.*[51] were employed for the double bond in oleoyl tails. While our previous work demonstrated that the parameters employed by Kukol[52] resulted in order parameters around the double bond that were in substantial disagreement with experiment[43], subsequent investigation has identified that Kukol did not correctly employ the parameters published by Bachar *et al.* Tests employing the correct Bachar parameters

for the double bond demonstrate minor improvements in the experimental agreement of the order parameters when compared to the original GROMOS-CKP simulations employing standard GROMOS parameters for the double bond[53].

Initial all-atom and coarse-grained structures were generated using PACKMOL[54]. All-atom structures were converted for use in united-atom simulations by removing non-polar hydrogen atoms, and for use with the ELBA force field using in-house scripts. To make the conversion from all-atom to united-atom systems as simple as possible for both this work and future studies, all of the united-atom lipid and cholesterol GROMACS topology files were modified to rearrange the atom order to match that of the corresponding CHARMM force field topologies. While somewhat laborious, such modifications to the topology files now enables trivial conversion of CHARMM all-atom membrane structures to simulation ready united-atom ones (e.g. through a single grep command) without the need for tools to alter the atom order of the structures.

Each system consisted of 128 total lipids and 4096 water molecules, or the equivalent number of water beads for CG systems. This is a higher level of hydration than conditions employed in the experiments that generated our reference data. However, we note that such a difference in hydration does not impact upon membrane properties or the determined x-ray scattering data[55–57]. Membranes consisted of mixtures of either DMPC, POPC, or DOPC and cholesterol across a range of 14 concentrations. Exact lipid compositions are described in the supplementary material. MARTINI systems used the DLPC lipid model, which also represents DMPC lipids owing to the lower coarse-grained resolution. The majority of the simulations were performed at lower cholesterol concentrations, where a negative partial-molecular area of cholesterol has been reported and the cholesterol condensing effect is at its strongest[8,11]. Five repeats were run per cholesterol concentration, each using independent starting structures. All simulations were performed using the 2018 series of the GROMACS simulation package[58], except for ELBA, which used LAMMPS (version 29 Oct 2020)[59].

Systems were minimized using the steepest descent algorithm for 5000 steps, before a 3-step equilibration process. During equilibration, a Berendsen thermostat[60] was used to maintain a temperature of 303.15 K (above the phase transition of all phospholipids tested here), using a coupling constant of 1.0 ps. A semi-isotropic Berendsen barostat[60] was used to maintain a pressure of 1 bar along the xy plane and z axis (the membrane plane and normal), with a coupling constant of 5.0 ps, and a compressibility of 4.5×10^{-5} bar^{-1}. Lipids and solvent were coupled to separate thermostats. Initially a NVT equilibration step of 0.25 ns was performed, followed by an NPT equilibration of 0.125 ns with a timestep of 1 fs. The timestep was increased to 2 fs for the final equilibration stage of 1 ns.

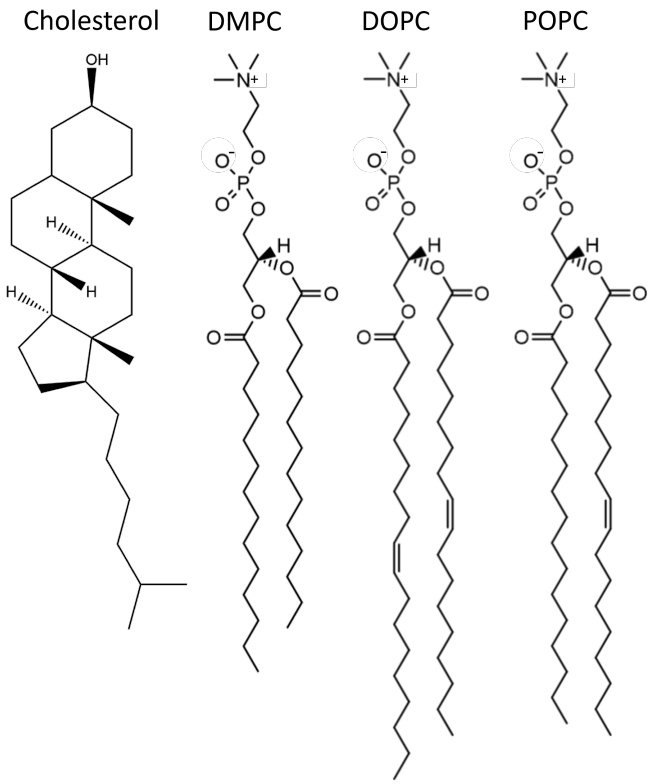

FIG. 1. The molecular structure of cholesterol, DMPC, DOPC, and POPC lipids.

The ELBA systems utilised a modified NVT equilibration protocol to eqilibrate the longer timestep. Initial NVT equilibration consisted of a timestep of 0.6 fs for 6 ps, followed by increasing the timestep to 1.2 fs and 2.0 fs for 120 ps and 500 ps. Subsequent equilibration in the NPT ensemble was identical to that used for other systems.

Production simulations were run for 200 ns, using the leap-frog integrator with a 2 fs time-step for all-atom systems, a 2 fs time-step for united-atom systems, 12 fs for MARTINI 2 systems, 20 fs for MARTINI 3, or a dual time-step of 2 fs and 6 fs for ELBA systems[61], which employed the rRESPA integrator[62]. The Nosè-Hoover thermostat[63] was used to maintain a temperature of 303.15 K with a time constant of 1.0 ps for all systems except MARTINI, which used the velocity rescale thermostat[64], as per published protocols[37–43,65]. A pressure of 1 bar was maintained using the Parinello-Rahman barostat[66], with a time constant of 5.0 ps for all systems except MARTINI 2 systems, which employed the Berendsen barostat, as per published protocols[37–43,65]. PME was used to solve long range electrostatic interactions, except for MARTINI and GROMOS systems which employed the reaction field method, as used in the original work publishing these force fields. In particular, GROMOS simulations employed a relative dielectric constant beyond the cut-off of 62, as applicable for SPC

water[67], while MARTINI simulations employed a relative dielectric constant of 15 within the cut-off and an infinite relative dielectric constant beyond. The LINCS algorithm was used to constrain all bonds involving hydrogen atoms, except for MARTINI systems, where LINCS was used to constrain all bonds. LINCS order and the number of iterations were set to 4 and 1 respectively for all simulations except those using the MARTINI 2 force field where values of 8 and 2 were used due to issues with energy conservation[68]. The remaining parameters were set to best match those used in the original publications, or parameters commonly used in the literature, and are outlined in table I. For GROMOS-CKP and GROMOS $53A6_L$ simulations, the settings employed for the cut-offs were those identified to most accurately reproduce the experimental properties of phospholipid membranes when performing simulations with the Verlet cut-off scheme, as employed in modern versions of the GROMACS software[53].

B. Analysis

1. Area per Lipid

The average area per lipid, a, was calculated from simulations by dividing the x-y area of the simulation box, $A_{\text{x-y}}$, by the number of lipid per leaflet, N_{leaflet}:

$$a(x) = \left\langle \frac{A_{\text{x-y}}}{N_{\text{leaflet}}} \right\rangle \tag{1}$$

Where $\langle ... \rangle$ represents the ensemble average, and a has been written as a function of the cholesterol mole fraction x, highlighting the effect of cholesterol on the membrane area. All analysis was performed using the last 50 ns of simulations only.

2. Condensation Analysis

The partial-molecular area of cholesterol, alongside several other cholesterol condensing parameters, are used for force field validation. These condensing parameters are calculated by fitting a model to the average area per lipid data of membranes across a range of cholesterol concentrations, and then calculating the derivatives of the curve for a given cholesterol concentration. Two models are discussed in this work, a model using a single non-linear equation, and another using two linear-equations. While all of these equations were originally derived by Edholm and Nagle[8], in the original publication only the non-linear equation model was used. The equations defining the models are introduced below.

We can define the average area per lipid of a binary mixture of a PC and cholesterol lipid as a mole fraction weighted average of the area per lipid of the individual components:

$$a(x) = (1-x)\hat{a}_{pc} + x\hat{a_{\text{chol}}} \tag{2}$$

where x is the cholesterol mole fraction, and $\hat{a}_{pc}$ and $\hat{a}_{\text{chol}}$ are constant lipid areas of the PC and cholesterol lipid respectively. Here, we use 'constant' to signify these values do not change with respect to cholesterol mole fraction. The constant PC lipid area can be calculated from a pure PC lipid membrane, while the constant area of cholesterol is more challenging to define, as cholesterol does not readily form a bilayer. While simple, equation 2 is inaccurate in its assertion that PC and cholesterol mixtures results in ideal mixing behaviour with respect to lipid areas. To address this approximation, one strategy is to replace the constant area terms with partial-molar area terms which would be functions of the cholesterol mole fraction. However, as the constant area formulation is enticing from an interpretive perspective, additional terms are instead added to equation 2, to capture the cholesterol condensing effect as characterised by a negative deviation from ideal mixing.

For low cholesterol concentrations, each cholesterol added to the membrane will condense the maximum possible number of neighbouring lipids, n, resulting in each of the neighbouring PC lipids having an area reduced by Δa:

$$a(x) = (1-x)\hat{a}_{pc} + x(\hat{a}_{\text{chol}} - n\Delta a) \tag{3}$$

The deviation from ideal mixing is captured by the remaining parameters, n and Δa, which quantify the reduction of membrane area per cholesterol molecule as caused by the condensing effect. n is the number of lipids which are condensed by a single cholesterol molecule, and Δa is the reduction in area associated with the condensing of a single PC lipid. Plotting $\frac{a(x)}{1-x}$ against $\frac{x}{1-x}$ yields a gradient given by $\hat{a}_{\text{chol}} = n\Delta a$, providing a graphical method for determining the partial molecular area of cholesterol[8,27].

For high cholesterol concentrations, each PC lipid will likely already neighbour a cholesterol molecule, resulting in all PC lipids being condensed, and thus each PC lipid will already have an area reduced by Δa. Adding an additional cholesterol molecule will increase the membrane area by the constant cholesterol area, $\hat{a}_{\text{chol}}$. Thus, in the limit of high cholesterol concentration the membrane area behaviour is governed by equation 4:

$$a(x) = (1-x)(\hat{a}_{pc} - \Delta a) + x\hat{a}_{\text{chol}} \tag{4}$$

Least squares regression was used to fit equations 3, and 4 to the area per lipid data. We note that while this model is termed the two linear-equation model, as both equations are fit simultaneously (i.e. as parameters are shared between equations, residuals are calculated across both equations and minimised simultaneously),

TABLE I. Parameters used in simulations.

Force field	LJ type	LJ cut-off / nm	Electrostatic type	Electrostatic cut-off / nm
CHARMM36	Force-switch	1.0 - 1.2	PME	1.2
Slipids	PME	1.0	PME	1.0
Lipid17	Cut-off[a]	1.0	PME	1.0
GROMOS $53A6_L$	Cut-off	1.0	Reaction Field	1.0
GROMOS-CKP	Cut-off	1.2	Reaction Field	1.2
MARTINI 2 & 3	Potential-shift	1.1	Reaction Field	1.1
ELBA	Force-switch	1.0	PME	1.2

[a] An additional dispersion correction was also included.

the model is in fact non-linear. Standard errors were estimated from the parameter covariance matrix using a linear approximation to the model function around the optimum[69].

The partial-molecular area of cholesterol $a_{\text{chol}}^{\text{pm}}$ may be calculated as the constant area of cholesterol $\hat{a}_{\text{chol}}$ minus how much it condenses the membrane:

$$a_{\text{chol}}^{\text{pm}} = \hat{a}_{\text{chol}} - n\Delta a \tag{5}$$

This corresponds to the intersect of the low cholesterol region linear equation (eq 3) with the ordinate $x = 1$, which is commonly how partial areas are calculated[8,10].

Finally, we note that previously a single non-linear equation was used to model the cholesterol condensing effect across the whole range of cholesterol concentrations, which is also derived by Edholm and Nagle[8]:

$$a(x) = c_0 + c_1 x + c_2(1-x)e^{-c_3 x} \tag{6}$$

where:

$$c_0 = \hat{a}_{pc} - \Delta a \tag{7a}$$

$$c_1 = \Delta a + \hat{a}_{chol} - \hat{a}_{pc} \tag{7b}$$

$$c_2 = \Delta a \tag{7c}$$

$$c_3 = n \tag{7d}$$

Further details on this single equation model can be found in[8].

C. Lipid Tail Order Parameters

Lipid acyl tail order parameters (S_{CH}) were calculated using the following equation:

$$S_{CH} = |\langle 3\cos^2\theta - 1\rangle/2| \tag{8}$$

where θ is the angle between the CH bond vector and the Z axis of the simulation cell. Order parameters were then averaged over CH bonds of both lipid tails and all PC lipids in the system. Lipid tail positions corresponding to carbon atoms involving double bonds were excluded as their corresponding order parameter values are very low, and therefore skew the comparison of DMPC to POPC and DOPC lipids.

III. RESULTS

Average lipid areas were calculated across a range of cholesterol concentrations for DMPC and DOPC membrane simulations, and used to fit the cholesterol condensing effect models. Initially, the single non-linear equation model equation (6) was fitted to the data. Two sets of experimental data report average lipid areas for DMPC and DOPC across a range of cholesterol concentrations: the data of Hung *et al.*[70], and the data of Pan *et al*[11]. Both experimental data sets were acquired from the original publications, using WebPlotDigitizer to extract numerical data from plots[71]. For experimental data sets from Pan *et al.* and Hung *et al.*, and the simulation data presented here, this single non-linear equation resulted in significant fitting issues, as is further discussed in Appendix A. As such, two linear-equations (eq 3 and 4), also derived by Edholm and Nagle[8], were used to model the area per lipid at limiting low and high cholesterol concentrations.

A. Two Linear-equation Model

Owing to the poor fitting behaviour of the single non-linear equation model (see appendix), equations 3 and 4 were fit to the lipid area data at low and high cholesterol concentration regions ($x < 0.2$ and $x > 0.3$). These cut-offs were chosen as they define the linear regions of the linear response of lipid area with respect to increasing membrane cholesterol content. The resulting fits are presented in figures 2 and 3 for DMPC and DOPC membranes, respectively. Experimental data from Hung *et al.*[70] and Pan *et al.*[11] are included in the analysis for comparison. However, the data from Pan *et al.* has only

4 observations, too few to fit this model. Parameters calculated from fitting the two linear-equation model to simulation and Hung *et al.* data are presented in the supplementary material (table S1).

Although the data of Pan *et al.* have too few data points to fit the two linear equation model, they have been included to provide a qualitative measure of experimental error. The experimental datasets appears to be more similar in DOPC membranes compared to DMPC membranes. For DMPC membranes, the inter-dataset difference appears to be largest in the cholesterol mole fraction region of 0.2 - 0.3, however there are no data from the Pan *et al.* dataset for cholesterol mole fractions above this range. Overall, the comparison between experimental datasets is limited in its ability to assess experimental error, highlighting the need for more experimental data over a wide range of cholesterol concentrations.

It is clear from the plots (figures 2 and 3), and the high R^2 values of the fits (see supplementary material, table S3 and S4) that the two linear fits are sufficient to model the lipid area data. As a means of validating the two linear-equation model in light of the poor fitting behaviour of the single non-linear equation model, we first analysed the results of fitting to experimental data from Hung *et al*[70]. In the case of the Hung *et al.* DMPC membrane data, the two linear fits predict a DMPC lipid area of 0.60 ± 0.00 nm^2, in excellent agreement with the data point at $x = 0$, and other literature values[11]. This indicates that the fit of the condensing effect parameters ($\hat{a}_{\text{chol}}$, Δa, and n) does not constrain the model to poorly predict the first data point.

For DOPC membranes, the two linear fits to the Hung *et al.* data predict a DOPC lipid area of 0.74 ± 0.00 nm^2, larger than other experimental values reported in the literature. Previously reported values, also at 30 °C, are 0.67 nm^2 [72], 0.72 nm^2 [11], 0.72 nm^2 [73], with the latter two values using the same X-ray methodology. It is somewhat concerning that the former, and arguably more reliable, DOPC area (0.67 nm^2), was calculated using a more robust joint X-ray and neutron refinement approach, as compared to relying only on X-ray data in the case of Hung et al. Despite this, the Hung et al. dataset is the only dataset available with sufficient observations spanning a range of cholesterol concentrations, and therefore is the only dataset which may be used as a benchmark for this analysis. Despite this, the lipid area predicted by the two linear fit method is consistent with the position of the first data point (which represents the DOPC area), suggesting that the divergence from other experimental values arises from the dataset of Hung *et al.*, and not the two linear-equation model per se.

The two linear fits suggest a partial-molecular area of cholesterol (a^{pm}_{chol}) of -0.06 ± 0.04 nm^2 for the Hung *et al.* DMPC membrane data. For DOPC membranes, a^{pm}_{chol} is predicted to be 0.03 ± 0.04 nm^2, significantly larger than that for DMPC membranes, in qualitative agreement with the literature[11].

The predicted constant area of cholesterol ($\hat{a}_{\text{chol}}$) for Hung *et al.* DMPC membranes is 0.38 ± 0.04 nm^2, falling within the experimental range of 0.3–0.4 nm^2[15,74,75]. However, for the DOPC membrane, the model predicts a slightly lower value of 0.35 ± 0.03 nm^2, despite the expectation of this method for $\hat{a}_{\text{chol}}$ to be independent of the degree of the condensing effect. The discrepancy between these values for DMPC and DOPC membranes is small, with each value falling within the standard deviation of the other.

Currently, there are no experimental literature values for the maximum number of lipids a single cholesterol molecule can condense (n), or by how much the area of a condensed lipids is reduced (Δa). However, the predicted values of 3.4 ± 0.4 and 0.13 ± 0.03 nm^2 for DMPC membranes, and 3.5 ± 0.5 and 0.09 ± 0.02 nm^2 for DOPC membranes, respectively, are all physically reasonable. The model predicts that a cholesterol molecule condenses approximately the same number of neighbouring lipids for both DMPC and DOPC membranes, with the differences in cholesterol condensation arising from by how much these lipids are condensed.

Overall, the two linear-equation model appears to adequately describe the data from Hung *et al.*, and the data from the simulations performed here, which both show linear behaviour in the low and high cholesterol concentration regions.

B. Force Field Comparison

Having validated the two linear-equation model with experimental data, the model was fitted to simulation data. Here, several force fields are tested in their ability to accurately reproduce experimental data, in terms of the cholesterol condensing effect parameters.

1. All-atom Force Fields

CHARMM36. The CHARMM36 force field predicts an a^{pm}_{chol} of -0.14 ± 0.01 nm^2 for DMPC membranes, the most negative of all of the force fields tested here, and indeed, slightly too negative compared to the fit to the experimental data of Hung *et al.*, which predicts a^{pm}_{chol} = -0.06 ± 0.04 nm^2.

The other condensing parameters predicted from the two linear-equation model allow further insight into differences between the CHARMM36 force field, and the experimental data of Hung *et al.* CHARMM36 predicts a cholesterol area ($\hat{a}_{\text{chol}}$) of 0.36 ± 0.01 nm^2, close to the experimental fit, which predicts 0.38 ± 0.04 nm^2. The average change in the area of a lipid associated with condensation (Δa) predicted by CHARMM36 is 0.16 ± 0.01 nm^2 which is slightly larger than the experimental fit, 0.13 ± 0.03 nm^2, but falls within one standard deviation. The final condensing parameter, the maximum number of lipids ordered by a cholesterol molecule (n) is predicted to be 3.1 ± 0.1, which is slightly smaller

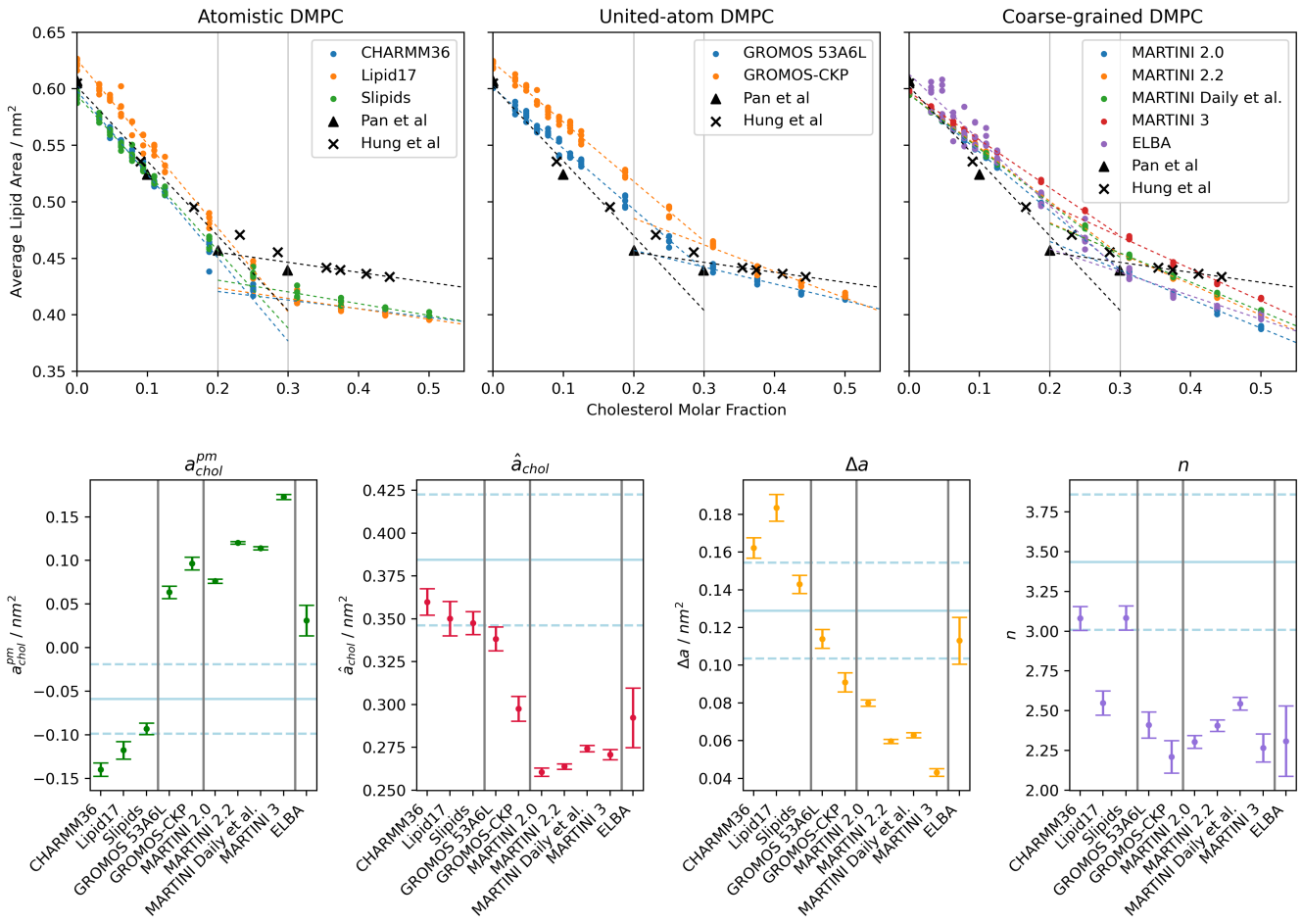

FIG. 2. Top: Average lipid area simulation data of DMPC cholesterol membranes (dots) were used to fit a cholesterol condensing model involving two linear-equations(dashed lines). Experimental data are shown with black crosses and triangles. Only the data of Hung *et al.* are used in the experimental two linear-equation model. Bottom: calculated cholesterol condensing parameters are also presented. Error bars represent one standard deviation. Fitted parameters from the experimental data of Hung *et al.* are also presented for comparison (solid blue line)(dashed blue line represents one standard deviation).

than the experimental value of 3.4 ± 0.4, but remains within one standard deviation. Overall, the CHARMM36 force field is in reasonable agreement with experiment, although small deviations from experimental values in all of the condensing parameters result in a larger (albeit still low) experimental deviation in the partial-molecular area of cholesterol.

For DOPC membranes, the value of $a^{pm}_{\rm chol}$ predicted by CHARMM36 is 0.13 ± 0.00 nm^2, which is too large compared to the experimental value of 0.03 ± 0.04 nm^2. CHARMM36 underestimates all of the remaining parameters, predicting values for $\hat{a}_{\rm chol}$, Δa, and n of 0.26 ± 0.00 nm^2, 0.05 ± 0.00 nm^2, and 2.4 ± 0.1 respectively, all falling below experimental values of 0.35 ± 0.03 nm^2, 0.09 ± 0.02 nm^2, and 3.5 ± 0.5. In particular, $\hat{a}_{\rm chol}$ falls below to the experimental range of 0.3–0.4 nm^2, and is also different from the value predicted for DMPC membranes. Differing values of $\hat{a}_{\rm chol}$ predicted in DMPC vs DOPC membranes is discussed later. Thus it would appear that too small values of Δa and n are partially compensated by a low value of $\hat{a}_{\rm chol}$, i.e. smaller values of Δa and n result in larger values of $a^{pm}_{\rm chol}$, while smaller values of $\hat{a}_{\rm chol}$ result in smaller values of $a^{pm}_{\rm chol}$. This results in a value of $a^{pm}_{\rm chol}$ which deviates less from the experimental value than the parameters used for its calculation. Thus, the CHARMM36 force field more accurately reproduces the cholesterol condensing effect in DMPC membranes as compared to DOPC membranes; this is the case for many of the force fields discussed below.

Slipids. Similar to the CHARMM36 force field, the Slipids force field is in good agreement with the DMPC data from Hung *et al.*, but performs less well for DOPC data. For DMPC membranes, Slipids predicts a $a^{pm}_{\rm chol}$ of -0.09 ± 0.01, more closely matching experiment compared to CHARMM36, and in the best agreement of all of the force fields tested here. Slipids predicts an $\hat{a}_{\rm chol}$ of 0.35 ± 0.01 nm^2, a Δa of 0.14 ± 0.00 nm^2, and an n of 3.1 ± 0.1, all in good agreement with the Hung

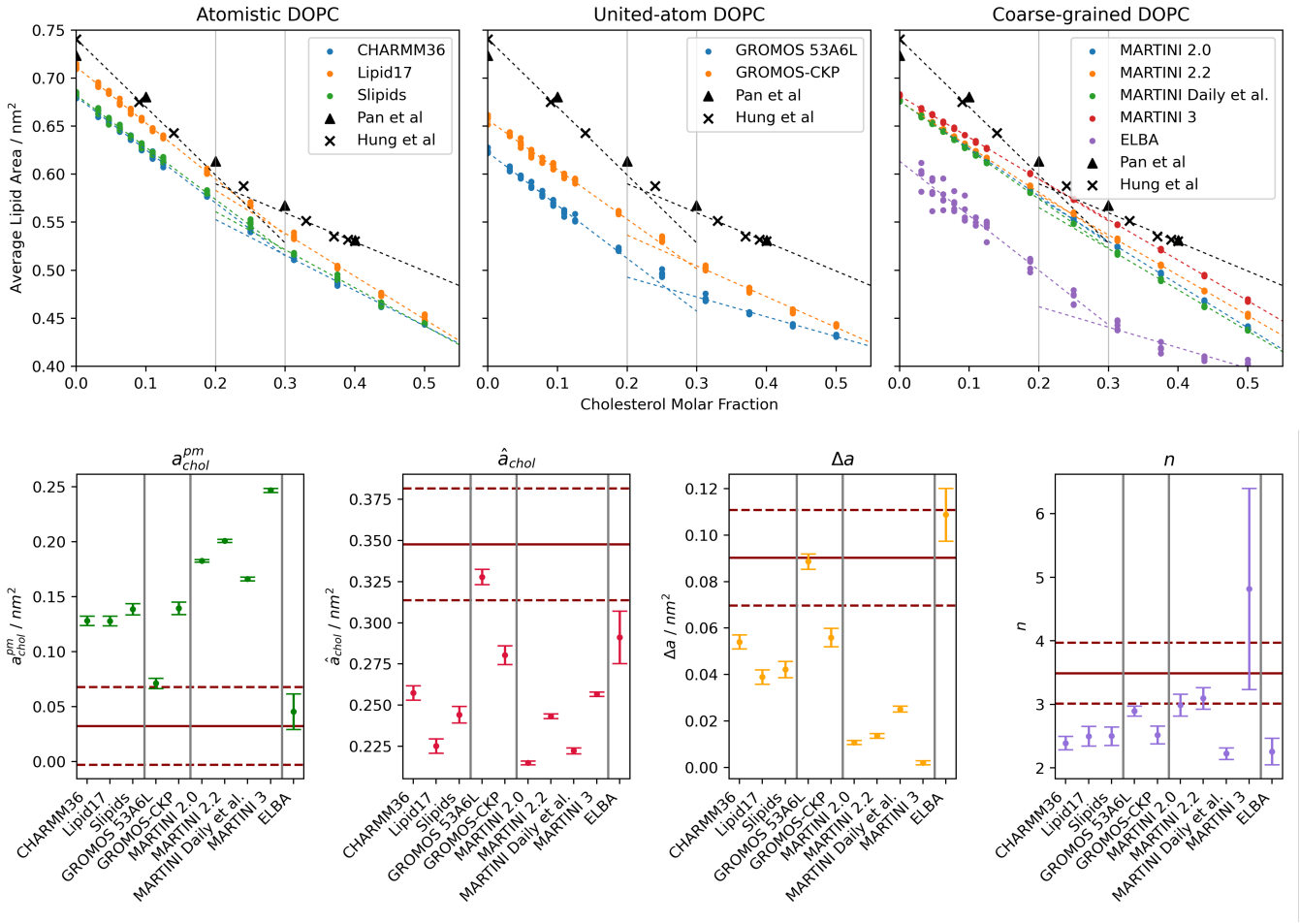

FIG. 3. Top: Average lipid area simulation data of DOPC cholesterol membranes (dots) were used to fit a cholesterol condensing model involving two linear-equations(dashed lines). Experimental data are shown with black crosses and triangles. Only the data of Hung *et al.* are used in the experimental two linear-equation model. Bottom: calculated cholesterol condensing parameters are also presented. Error bars represent one standard deviation. Fitted parameters from the experimental data of Hung *et al.* are also presented for comparison (solid red line)(dashed red line represents one standard deviation).

et al. data and marginally out-performing CHARMM36 for values of Δa and n. Overall, for DMPC membranes, Slipids is a slight improvement on CHARMM36, representing the best performing force field studied here in its ability to predict cholesterol condensing parameters of DMPC membranes.

For DOPC membranes, the Slipids force field performs less well compared to DMPC membranes, and predicts condensing parameters similar to CHARMM36. Slipids predicts $a^{pm}_{\mathrm{chol}} = 0.14 \pm 0.01$ nm^2, too large compared to experiment. Additionally, Slipids predicts $\hat{a}_{\mathrm{chol}} = 0.24 \pm 0.01$ nm^2, $\Delta a = 0.04 \pm 0.00$ nm^2, and $n = 2.5 \pm 0.1$, all too small compared to experiment. Again, the small values of Δa and n are partially compensated by a small value of $\hat{a}_{\mathrm{chol}}$, but not enough to bring a^{pm}_{chol} more inline with experiment. For DOPC membranes, the Slipids force field results are similar to, but slightly worse than, CHARMM36, with the main sources of error coming from values of $\hat{a}_{\mathrm{chol}}$ and Δa.

Lipid17. Upon initial inspection, the Lipid17 force field performs similarly to the CHARMM36 and Slipids force fields for DMPC membranes, predicting $a^{pm}_{\mathrm{chol}} =$ -0.12 $\pm$ 0.01 nm^2, in between values predicted by CHARMM36 and Slipids. Additionally, Lipid17 predicts $\hat{a}_{\mathrm{chol}} = 0.35 \pm 0.01$ nm^2 lying inside the experimental range. However, Lipid17 deviates from experiment for values of $\Delta a = 0.18 \pm 0.01$ nm^2 and $n = 2.5 \pm 0.1$, which are too high and too low respectively. Deviations in these values are in opposite directions, and thus, they have opposite impacts on a^{pm}_{chol}, which largely cancel. This results in Lipid17 predicting a value of a^{pm}_{chol} similar to CHARMM36 and Slipids despite under-performing both in terms of reproducing Δa and n. This highlights the utility of calculating cholesterol condensing parameters in addition to partial-molecular areas.

For DOPC, Lipid17 predicts condensing parameters very similar to CHARMM36 and Slipids, with the only difference being that Lipid17 predicts $\hat{a}_{\mathrm{chol}} = 0.23 \pm$

0.00 nm^2, which is too small compared to experiment and slightly smaller than values form CHARMM36 and Slipids.

2. United-Atom Force Fields

GROMOS 53A6$_L$. For DMPC membranes, the GROMOS 53A6$_L$ force field predicts a^{pm}_{chol} to be 0.06 ± 0.01 nm^2, which is positive, and deviates from the experimental value more than any of the all-atom force fields studied. GROMOS 53A6$_L$ predicts a constant cholesterol area , $\hat{a}_{chol}$, of 0.34 ± 0.01 nm^2, in good agreement with the experimental value of 0.38 nm^2, and also predicts Δa = 0.11 ± 0.00 nm^2, which is smaller than the experimental value of 0.13 ± 0.03 nm^2, but within one standard deviation. For n, the GROMOS 53A6$_L$ force field deviates more from experiment, predicting 2.4 ± 0.1, significantly smaller than the experimental value of 3.4 ± 0.4.

For DOPC membranes, the GROMOS 53A6$_L$ force field predicts a a^{pm}_{chol} value of 0.07 ± 0.00 nm^2, which is too large compared to the experimental value of 0.03 ± 0.04 nm^2, but is an improvement compared to the all-atom force fields studied here. Furthermore, GROMOS 53A6$_L$ predicts $\hat{a}_{chol}$ = 0.33 ± 0.00 nm^2, which is slightly too small compared to the experimental value of 0.35 ± 0.03 nm^2. Finally, GROMOS 53A6$_L$ predicts Δa = 0.09 ± 0.02 nm^2, identical to the experimental value, and n = 2.9 ± 0.1 which is too small compared to experiment. While GROMOS 53A6$_L$ slightly under-predicts the cholesterol condensing effect in DOPC membranes, the remaining condensing parameters are in good experimental agreement. Overall, GROMOS 53A6$_L$ underestimates the magnitude of the cholesterol condensing effect in DMPC membranes, but is in relatively good agreement with DOPC membranes, improving on all-atom models in this regard. For both lipid types, the main source of error lies in under-predicting the number of lipids condensed by a single cholesterol molecule.

GROMOS-CKP. Despite being in the GROMOS family of force fields, and employing the same cholesterol model, GROMOS-CKP differs from GROMOS 53A6$_L$ in terms of this cholesterol condensing effect analysis. For DMPC membranes, GROMOS-CKP predicts a^{pm}_{chol} = 0.10 ± 0.01 nm^2, and $\hat{a}_{chol}$ = 0.30 ± 0.01 nm^2, Δa = 0.09 ± 0.01 nm^2 and n = 2.2 ± 0.1, all deviating more from the Hung *et al.* values compared to the GROMOS 53A6$_L$ force field. Thus the GROMOS-CKP force field slightly under-performs the GROMOS 53A6$_L$ for DMPC membranes, with a low predicted value of $\hat{a}_{chol}$ partially compensated by low predicted values of Δa and n.

For DOPC membranes, the GROMOS-CKP force field predicts a^{pm}_{chol} to be 0.14 ± 0.01 nm^2, deviating from the experimental value more than GROMOS 53A6$_L$. The value of $\hat{a}_{chol}$ predicted by GROMOS-CKP is 0.28 ± 0.01 nm^2 falling under the experimental range of 0.3 − 0.4 nm^2, but similar to the value predicted by GROMOS-CKP in DMPC membranes, in contrast to many of the other force fields studied here. GROMOS-CKP predicts a value of Δa, of 0.06 ± 0.00 nm^2 which is in good agreement with the experimental value, but still deviates more than GROMOS 53A6$_L$, and also predicts a n = 2.5 ± 0.1, which is significantly lower than the experimental value. Similarly to its performance for DMPC membranes, for DOPC membranes GROMOS-CKP performs worse than GROMOS 53A6$_L$, with a small value of $\hat{a}_{chol}$ partially compensating for small Δa and n values. If the force field more accurately predicted the constant area of cholesterol with no other modification, it would overall perform worse in regards to capturing the cholesterol condensing effect.

3. Coarse-grained Force Fields

MARTINI 2. Three cholesterol models were tested with the MARTINI 2 force field: the old MARTINI 2.0 cholesterol model[44] (denoted MARTINI 2.0) a newer MARTINI 2.2 cholesterol model incorporating virtual sites to add asymmetry to the molecule[45] (denoted MARTINI 2.2) and a model published by Daily *et al.*[21] further increasing the asymmetry and resolution of the model by using smaller beads (denoted MARTINI Daily *et al.*). Overall, the MARTINI force field, irrespective of which cholesterol model is used, performs the least well as compared to the other force fields studied here. For both DMPC and DOPC membranes, the MARTINI force field significantly under-predicts the magnitude of the cholesterol condensing effect.

For DMPC membranes, the MARTINI 2.0 force field predicts the lowest value of a^{pm}_{chol} of 0.08 ± 0.00 nm^2, compared to 0.12 ± 0.00 nm^2 and 0.11 ± 0.00 nm^2 as predicted by MARTINI 2.2 and MARTINI Daily *et al.*, respectively. Interestingly, all of the MARTINI cholesterol models predict similar values of $\hat{a}_{chol}$, with MARTINI 2.0 and 2.2 predicting a value of 0.26 ± 0.00 nm^2, while MARTINI Daily *et al.* predicts a value of 0.27 ± 0.00 nm^2. All of these values lie below the experimental range of 0.3–0.4 nm^2. Additionally the MARTINI models also predict similar values of Δa, with the MARTINI 2.0 model predicting 0.08 ± 0.00 nm^2, and MARTINI 2.2 and Daily *et al.* both predicting 0.06 ± 0.00 nm^2, all significantly lower than the experimental value of 0.13 ± 0.03 nm^2. The models predict slightly different values for n; MARTINI 2.0 predicts 2.3 ± 0.00, MARTINI 2.2 predicts 2.4 ± 0.00, and MARTINI Daily *et al.* predicts 2.5 ± 0.00. These values of n are similar to values predicted by the united-atom force fields, and are too small compared to experiment, 3.4 ± 0.4. For DMPC membranes, the MARTINI cholesterol models tested here are in overall poor agreement with experiment, all predicting values of a^{pm}_{chol} significantly larger than experiment. This is caused by the cholesterol molecules only slightly condensing neighbouring lipids as suggested by the low Δa value. Additionally, the values of a^{pm}_{chol} are artificially

low, caused by the cholesterol models being un-physically small compared to experiment.

For DOPC membranes, the MARTINI cholesterol models are again in poor agreement with the Hung data, suffering from the same issues of predicting values of $\hat{a}_{\text{chol}}$, Δa, and n which are all significantly smaller than the experimental Hung *et al.* data, while predicting values of a^{pm}_{chol} which are too large.

Overall, the MARTINI 2 force field and cholesterol models tested here poorly captures the cholesterol condensing effect, predicting values of a^{pm}_{chol} too large for both DMPC and DOPC membranes. This deviation from experimental data would be even greater if the MARTINI cholesterol models had a larger, more accurate area. Small values of Δa, and n suggest the MARTINI cholesterol models have a relatively small impact on neighbouring lipids, condensing too few by an ammount which is too small.

MARTINI 3. The MARTINI 3 force field has undergone significant re-parameterisation compared to MARTINI 2. Both PC lipids[47] and cholesterol[46] have updated topologies and parameter sets to take advantage of the new bead selection available in MARTINI 3. For DMPC membranes, MARTINI 3 predicts $a^{pm}_{\text{chol}} = 0.17 \pm 0.00$ nm, deviating from experiment more than any of the MARTINI 2 cholesterol systems. MARTINI 3 predicts $\hat{a}_{\text{chol}} = 0.27 \pm 0.00$ nm^2, smaller than experiment and similar to values predicted by MARTINI 2. Interestingly, the MARTINI 3 system predicts Δa to be 0.04 ± 0.00 nm^2, significantly lower than both experiment and what is predicted by MARTINI 2. Finally, MARTINI 3 predicts n to be 2.3 ± 0.01, which is too small compared to experiment but similar to values predicted by MARTINI 2.

For DOPC membranes, MARTINI 3 predicts $a^{pm}_{\text{chol}} = 0.25 \pm 0.00$ nm ^{2}, again too large compared to experiment and larger than MARTINI 2 predictions. MARTINI 3 predicts $\hat{a}_{\text{chol}} = 0.26 \pm 0.00$ nm^2, which is too small compared to experiment, but is larger than predicted by MARTINI 2, and thus an improvement. Interestingly MARTINI 3 predicts the largest value of n for DOPC membranes (4.8 ± 1.6), which is too large compared to experiment. The relatively high error of n likely comes from the value of $\Delta a = 0.00 \pm 0.00$ allowing increased freedom in n during the fitting. Overall, MARTINI 3 appears to model the cholesterol condensation effect less accurately compared to MARTINI 2.

ELBA. The ELBA force field is set up in a dual-resolution configuration, using an all-atom model for cholesterol, specifically the CHARMM36 model, and coarse-grained model for the PC lipid. For DMPC membranes, the ELBA force field predicts a a^{pm}_{chol} value of 0.03 $\pm$ 0.02 nm^2, which is too large compared to experiment. Interestingly, ELBA's prediction of a^{pm}_{chol} is an improvement on the united-atom GROMOS force fields, but not as good as the all-atom force fields. The value of $\hat{a}_{\text{chol}}$ predicted by ELBA is 0.29 ± 0.02 nm^2, marginally outside of the experimental range of $0.3 - 0.4$ nm^2. ELBA predicts a value of $\Delta a = 0.11 \pm 0.01$, in fair agreement with experiment, and a value of $n = 2.3 \pm 0.2$, which is too small.

It is noteworthy that ELBA uses the CHARMM36 cholesterol model, but predicts a different value of $\hat{a}_{\text{chol}}$. From the plot of the fit in figure 2, it can be observed that for the ELBA force field, the area per lipid is not linear with respect to the cholesterol mole fraction for mole fractions above 0.3. Owing to this, the two linear-equations were refit using only the data above 0.35, where the three remaining datapoints exhibit linear behaviour. The resulting fit has no change in a^{pm}_{chol}, but differs in the remaining parameters, (see supplementary material table S3, denoted as ELBA ($x > 0.35$)). The new value of $\hat{a}_{\text{chol}}$ (0.32 ± 0.03 nm^2) has been brought significantly closer to the CHARMM36 value (0.36 ± 0.01 nm^2), with the remaining difference possibly caused by differences in packing behaviour of the cholesterol model in the coarse-grained ELBA lipid environment compared to the all-atom CHARMM36 environment. The updated fit predicts $\Delta a = 0.13 \pm 0.02$ nm^2, matching the experimental value, but predicts $n = 2.1 \pm 0.2$, significantly lower than experiment. ELBA also introduces scaling factors into the mixing rules for interactions between the all-atom and coarse-grained subsystems, affecting the Lennard-Jones interactions and thus the bead/atom sizes. Overall, for DMPC membranes, the ELBA force field predicts that cholesterol orders too few neighbouring lipid molecules.

In the case of DOPC membranes, ELBA predicts $a^{pm}_{\text{chol}} = 0.05 \pm 0.02$ nm^2, and is in the best agreement with the experimental value compared to the other force fields studied here. ELBA predicts $\hat{a}_{\text{chol}} = 0.29 \pm 0.02$ nm^2 in DOPC membranes, just under the experimental range of 0.3–0.4 nm^2, and this time larger than the value predicted by CHARMM36. Finally, ELBA predicts values of $\Delta a = 0.11 \pm 0.01$ nm^2 in fair agreement with experiment, but too large, and $n = 2.3 \pm 0.2$, significantly lower than experiment. For DOPC membranes ELBA is in fair agreement with experimental data, but predicts the constant cholesterol area, and the number of lipids ordered by cholesterol to be too small. Overall the performance of ELBA in capturing the cholesterol condensing effect is more similar to the united-atom force fields tested here, out-performing MARTINI, but underperforming against the all-atom force fields.

C. POPC Cholesterol Containing Membranes

POPC-cholesterol systems were simulated owing to POPC having tail saturation character between that of DMPC and DOPC, with the aim that this may offer additional insight into the role of saturation on the cholesterol condensing effect. As there are no experimental data characterising POPC-cholesterol membrane areas over a range of cholesterol concentrations for validation, only all-atom POPC-cholesterol simulations were performed, owing to these force fields previously performing the most

consistently accurate. While GROMOS 53A6$_L$ performs more accurately for DOPC membranes, it fails to predict a negative value of a_{chol}^{pm} for DMPC membranes. The two linear-equation model was fitted to the lipid area data, and results are presented in figure 4, and table S5 of the supplementary material. For each force field, the corresponding parameters from fits to DMPC and DOPC membranes are included for comparison.

The condensing parameters for POPC membranes overall suggest that the cholesterol condensing effect behaviour in POPC membranes lies somewhere in between that of DMPC and DOPC membranes. All three of the all-atom force fields predict positive values of a_{chol}^{pm} close to 0, which are slightly more similar to values reported for DOPC membranes. The remaining parameters all show similar behaviour, falling in between values obtained from the corresponding DMPC and DOPC fits, with a skew towards the DOPC data. The exception is that Lipid17 and Slipids predict values of n for POPC membranes which are lower than the DOPC values.

The comparison of parameters between membrane types, in figure 4, also highlights the differences in $\hat{a}_{\mathrm{chol}}$. The fitted model aims for $\hat{a}_{\mathrm{chol}}$ to be constant and independent of the membrane composition. While the fits to the experimental data of Hung *et al.* yield similar values of $\hat{a}_{\mathrm{chol}}$ in DMPC and DOPC membranes; this is clearly not the case for the simulation data.

D. Constrained $\hat{a}_{\mathrm{chol}}$ Model

During the fitting of the two linear-equations to DMPC and DOPC data, it was observed that the area of cholesterol ($\hat{a}_{\mathrm{chol}}$) differed between the different membranes. In theory, this should not be the case, with n and Δa varying to accommodate for differences in cholesterol condensing behaviour between lipid types. The two linear fits consistently predict smaller values of $\hat{a}_{\mathrm{chol}}$ in DOPC membranes compared to DMPC membranes, with the DOPC values regularly falling under the experimental range 0.3–0.4 nm^2. In an attempt to reconcile these differences, the two linear-equation model was refit to the DOPC data, while constraining $\hat{a}_{\mathrm{chol}}$ to the value predicted from the DMPC membrane. The constrained $\hat{a}_{\mathrm{chol}}$ fits are presented in figure 5, and fit parameters are listed in table S6 of the supplementary material.

For the all-atom force fields, the fits to the low cholesterol region remain largely unaltered, aligning well with the data. Conversely, for the high cholesterol concentration region, the constrained fits are less well aligned with the underlying lipid area data, with the model predicting a too shallow gradient than suggested by the data, as can be observed in figure 5(top) and from the increase in mean absolute error (MAE) associated with the constrained fit (see supplementary material table S6). Interestingly, for the united-atom, and coarse-grained force fields, this issue is less pronounced, with a reasonable agreement with the underlying data points across the full range.

We note that constraining values of $\hat{a}_{\mathrm{chol}}$ has little impact on the resulting values of a_{chol}^{pm}, with the other condensing parameters shifting to offset the imposed change in $\hat{a}_{\mathrm{chol}}$. The changes in condensing parameters are most pronounced for the all-atom force fields, which result in increased values of Δa, but decreased values of n. As the decrease of n is of a larger magnitude compared to Δa, this also compensates for the increase in $\hat{a}_{\mathrm{chol}}$, rationalising the consistency of a_{chol}^{pm} values between constrained and unconstrained fits.

These results suggest that the predicted values of a_{chol}^{pm} are relatively insensitive to the exact value of $\hat{a}_{\mathrm{chol}}$, with the other cholesterol condensing parameters adjusting to compensate. The low sensitivity to the underlying parameters is favourable behaviour and allows for increased confidence in the predicted values of a_{chol}^{pm} as the differences in the underlying parameters only have a small impact.

E. Average Lipid Tail Order Parameters

Increased lipid tail order is believed to be central to the mechanism of cholesterol condensation, in which each cholesterol imposes order on neighbouring PC lipids[76]. To further investigate the cholesterol condensing effect in PC membranes, lipid acyl tail order parameters were calculated and averaged over each carbon and each tail for a given cholesterol concentration, and are presented in figure 6. Experimental POPC order parameters from[77] (extracted from the paper using webplotidigizer[71]) are also included in figure 6. This analysis was only performed for all-atom simulations, which best reproduce experimental data and contain hydrogen positions required for order parameter calculation.

For DMPC, POPC, and DOPC membranes, there is a positive correlation between the average lipid tail order parameter and cholesterol concentration. This agrees with the theory that cholesterol molecules impose order on neighbouring PC lipid molecules. Interestingly, there is a clear difference in the lipid tail order parameter behaviour of each lipid.

In the case of DMPC membranes, there is a steep increase in the averaged order parameter from $x = 0$ to $x = 0.3$, at which point the values plateau to a value of approximately 0.35. For DOPC membranes a much shallower increase is observed across the whole range of cholesterol concentrations tested, with no notable plateau.

POPC membranes have an average lipid tail order parameter character somewhat in between that of DMPC and DOPC. A steady increase is observed across the majority of the cholesterol concentration range until $x = 0.45$, at which point, a plateau begins to be observed, with the average order parameters reaching a final value of approximately 0.275, in between values observed at similar cholesterol concentrations for DMPC and DOPC

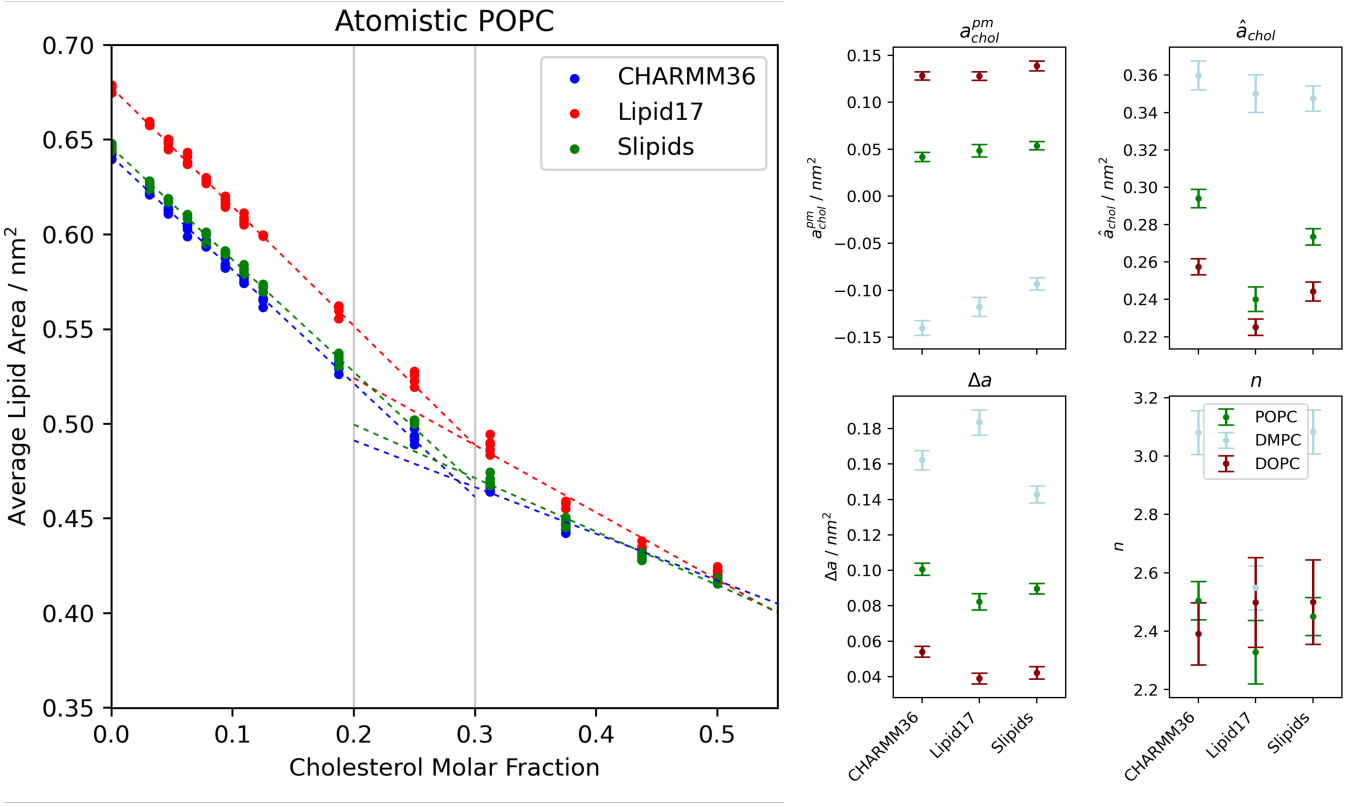

FIG. 4. Left: Average lipid area simulation data of POPC cholesterol membranes (dots) were used to fit a cholesterol condensing model involving two linear fits (dashed lines). Right: calculated cholesterol condensing parameters are also presented. Datapoints for the corresponding parameters of DMPC (light blue) and DOPC (dark red) membranes are included for comparison. Error bars show one standard deviation.

membranes. The simulation averaged order parameters are in good experimental agreement across the cholesterol range tested, with the largest discrepancy occurring at a cholesterol mole fraction of approximately 0.35. Among the force fields included in this analysis, Slipids shows the best agreement with experimental results. For a more detailed comparison of simulation and experimental POPC cholesterol order parameters, see[36].

IV. DISCUSSION

Several lipid force fields have been assessed in their ability to capture the cholesterol condensing effect in terms of recreating experimental cholesterol condensing parameters, including the partial-molecular area of cholesterol. A two linear-equation model used here differs from a previously used model involving a single non-linear equation, despite all equations being derived in the same publication[8]. The use of the two linear-equation model was necessitated in this work due to the poor fitting behaviour of the single non-linear equation model. Although the two linear-equation model offers significantly improved fitting behaviour, it is limited by its calculation of only two gradients, which only predict two partial-molecular areas of cholesterol: one at high and one at low cholesterol concentrations. Despite this, the two linear-equation model is sufficient to model these regions, in which the average area per lipid shows a linear response to increasing cholesterol content. Furthermore, fitting the two linear-equation model to the experimental data of Hung *et al.* results in parameters which are physically plausible. We note that a limitation of the analysis employed here is the lack of robust experimental data over a range of cholesterol concentrations. While the data used are from X-ray experiments, they diverge from observations using more robust joint X-ray and neutron refinement schemes[72]. Furthermore, more observations over the entire cholesterol range of interest here, would allow for better refinement of low and high limiting cholesterol behaviour. Comparison of the fitted parameters of cholesterol condensing models allows the analysis to include all data points from both simulation and experimental datasets, but the reliance on experimental lipid areas derived from X-ray experiments comes with a set of assumptions[72,78]. To address this concern, we also provide direct comparison between simulation and experimental X-ray form factors[11] in the appendix. Overall, the form factor analysis we perform offers more mixed results compared to the area analysis. We believe this may

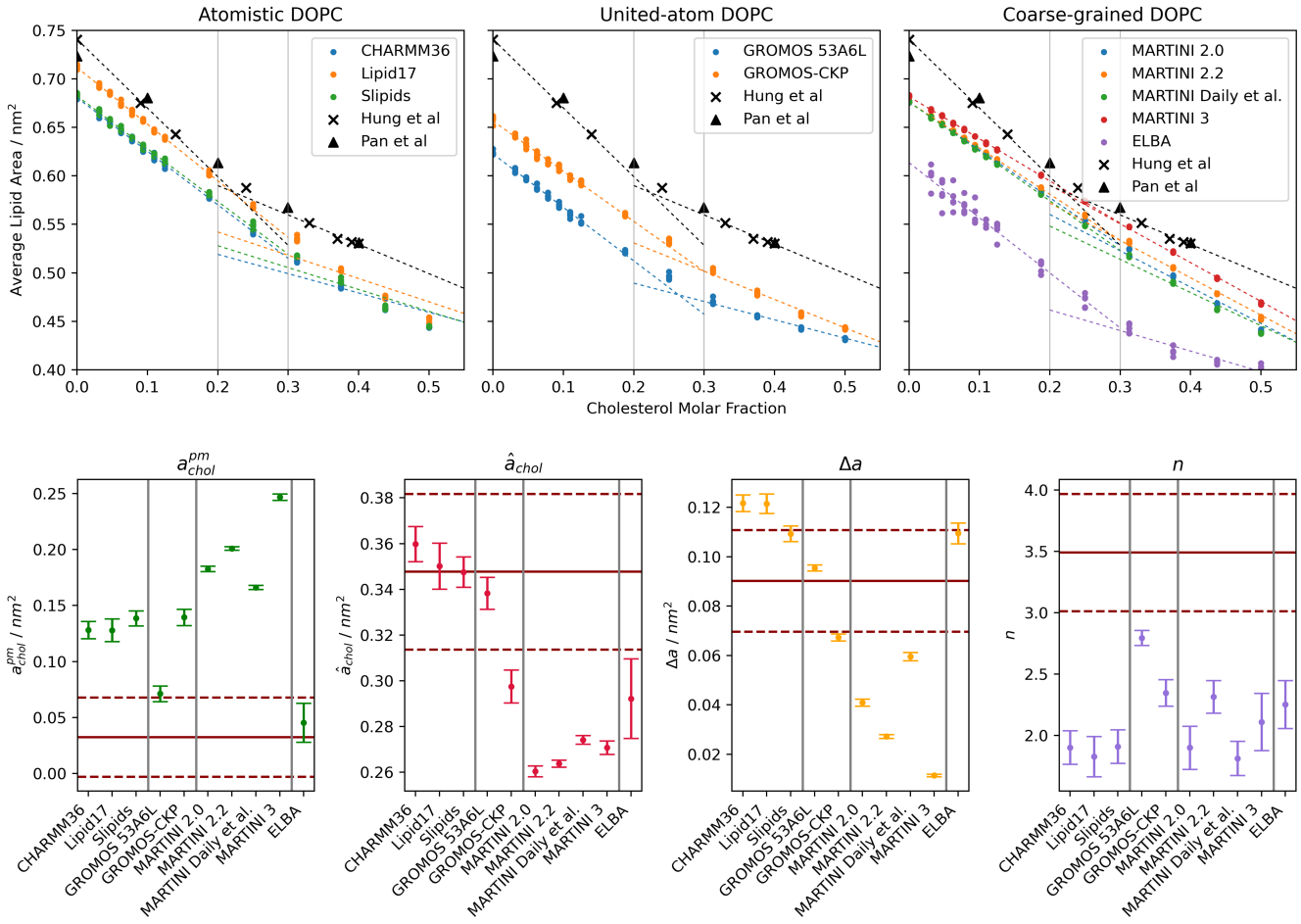

FIG. 5. Constrained $\hat{a}_{\mathrm{chol}}$ results. Top: Average lipid area simulation data of DOPC cholesterol membranes (dots) were used to fit a cholesterol condensing model involving two linear fits (dashed lines). Bottom: calculated cholesterol condensing parameters are also presented. The experimental data of Hung *et al.* is also presented for comparison (solid red line)(dashed red line represents one standard deviation of the value obtained by fitting to the experimental data). Error bars represent one standard deviation.

be caused, in part, by the small amount of experimental form factor data available, at only two data points each for DMPC and DOPC lipids. This point is discussed further in the appendix, again highlighting the need for more experimental data.

An issue observed with the two linear-equation model was that it would produce different values of the constant area per cholesterol ($\hat{a}_{\mathrm{chol}}$) parameter for different membranes. The model was derived with the aim that $\hat{a}_{\mathrm{chol}}$ should remain constant, with the other model parameters adjusting to account for differences in the cholesterol condensing effect for different membranes. Despite this, constraining the values of $\hat{a}_{\mathrm{chol}}$ has little effect on predicted values of the partial-molecular area of cholesterol, allowing for greater confidence in these values. Lipid acyl tail order parameters may offer additional insight into this issue. As reported here, the increase in order parameters with increasing cholesterol concentration is dependent upon the saturation character of the lipid tails, and thus cholesterol imposes order on DMPC, POPC, and DOPC lipids to different extents. Specifically, while order parameters plateau at approximately $x = 0.35$ for DMPC membranes, this plateau is observed at $x = 0.45$ for POPC, and not at all for DOPC membranes. As such, while the assumption that additional cholesterol condensation is absent at high cholesterol concentrations is true for DMPC, order parameters suggest this is not the case for DOPC membranes. Thus, the cut-off values for low and high cholesterol regions may need refining for different lipid types. While this study focused on simulations within the low cholesterol concentration region, further data are required in the high and middle cholesterol concentration regions to better characterise the cholesterol condensing effect, and further refine the two linear-equation model. While lipid tail order parameters are an alluring target for force field validation, there is an unfortunate lack of experimental data across a range of cholesterol concentrations, as required for such work.

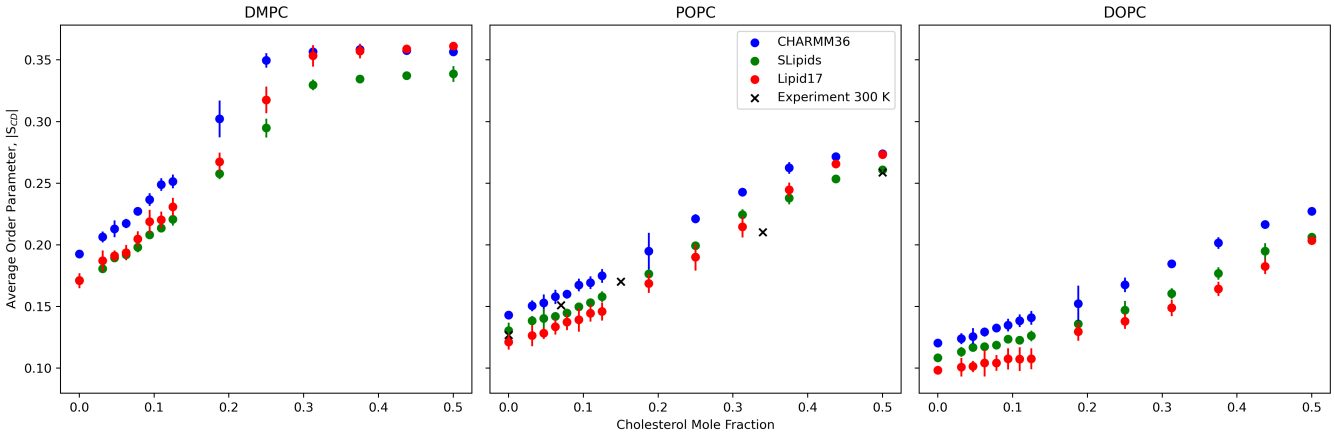

FIG. 6. Average lipid tail order parameters of all-atom simulations of cholesterol containing membranes. The average was taken over each carbon in each acyl tail. Experimental data for the POPC-cholesterol systems from[77] are depicted with Xs. Tail positions corresponding to double bonded carbon atoms were excluded from averaging.

The ELBA force field may offer a unique insight into how force fields capture the cholesterol condensing effect. Despite being a coarse-grained force field, ELBA boasts a significant improvement in accuracy compared to the MARTINI force field with respect to reproducing experimental cholesterol condensing parameters. Indeed, there are several fundamental differences in the philosophy of these force fields which may lead to such differences: i) ELBA has a lower degree of coarse-graining compared to MARTINI, especially in the water mapping, ii) ELBA systems are dual resolution, with the PC lipids modelled at the coarse-grained level and cholesterol modelled at the all-atom level, and iii) ELBA implements a more realistic electrostatic model compared to MARTINI. It is hard to evaluate which of these properties contribute the most to the improvements associated with ELBA. However, the increased resolution of the all-atom cholesterol molecule will facilitate the asymmetry of the cholesterol model, which is thought to be crucial to the cholesterol condensing effect[76].

Interestingly, GROMOS 53A6$_\mathrm{L}$ and GROMOS-CKP yield different cholesterol condensing parameters, despite employing the same cholesterol model. This highlights that lipid parameters also play a crucial role in condensation. We propose that the difference in condensing behaviour between the two force fields is likely due to the larger radius of the carbonyl carbon atom type (CH0) in GROMOS-CKP compared to that in GROMOS 53A6$_\mathrm{L}$ (C).

Furthermore, differences between MARTINI 2 and 3 may offer additional insight into the ability of a force field to capture the cholesterol condensing effect. The MARTINI 3 cholesterol model increases asymmetry by incorporation of the new *tiny* bead to model two methyl groups of the rough face of cholesterol, in addition to more accurately capturing cholesterol-lipid interactions, as shown by recreating all-atom 2-dimensional radial distribution functions of lipids surrounding cholesterol molecules[46]. Interestingly, despite these improvements, the analysis presented here suggests MARTINI 3 captures the cholesterol condensing effect less accurately compared to MARTINI 2. Thus it would appear that improved recreation of the surrounding PC lipid distribution and increasing cholesterol asymmetry are not universal targets for improving cholesterol models. Despite this, we note that molecule topologies and parameters are complex and there is likely a large interplay of parameters driving this phenomenon which may not be easily assessed independently. Further analysis of MARTINI 2 and MARTINI 3 systems may allow the determination of molecular features which bring about cholesterol condensation.

Overall, the analysis presented here suggests that the force field type (all-atom vs united-atom vs coarse-grained) is a reasonable predictor of the accuracy with which the cholesterol condensing effect is captured. We report that all-atom force fields most consistently capture the cholesterol condensing effect when considering both DMPC and DOPC membranes, however the GROMOS 53A6$_L$ force field is most accurate for DOPC membranes at the expense of poor accuracy for DMPC membranes. Comparatively the coarse-grained force fields capture the condensing effect less well. It has been previously suggested that the asymmetry between the two faces of cholesterol, specifically the methyl groups protruding from the planar sterol region, plays an important role in the cholesterol condensing effect[76]. As such the increased resolution of the methyl groups in the all-atom force fields may play an important role in capturing the cholesterol condensing effect. Despite this, the increase in asymmetry and resolution associated with the Daily *et al.,* MARTINI cholesterol model compared to the other MARTINI 2 models tested, offers no significant increase in the force field's accuracy, and indeed, although MARTINI 3 has a more asymmetric cholesterol model, it performed less well in this analysis compared to MAR-

TINI 2. Finally, the data presented here suggests that the CHARMM36 and Slipids force fields best capture the cholesterol condensing effect in DMPC membranes, with Slipids capturing the cholesterol condensing effect in DMPC membranes with slightly better accuracy at the expense of a slightly worse accuracy in DOPC membranes, compared to CHARMM36. For DOPC membranes, our results show that the GROMOS $53A6_L$ force field is in best agreement with experiment.

V. CONCLUSION

To conclude, we have studied the ability of several commonly used lipid force fields to accurately reproduce the cholesterol condensing effect. Our results highlight the utility in calculating cholesterol condensing parameters for a more rigorous analysis compared to only reporting partial-molecular cholesterol areas, and reveal that the all-atom force fields studied here best capture cholesterol condensation in DMPC membranes. Specifically the CHARMM36 or Slipids force fields are recommended for DMPC membranes, while GROMOS $53A6_L$ is recommended for DOPC membranes, owing to their accuracy in reproducing cholesterol partial-molecular areas, and cholesterol condensing parameters. While the analysis presented here considers simple model membranes, the cholesterol condensing effect holds crucial implications for larger, biologically relevant systems. For example, as lipid raft formation is thought to stem from the cholesterol condensing effect[79], simulations studying lipid rafts should use force fields which properly capture the this effect. Furthermore, as the cholesterol condensing effect alters membrane thickness, we highlight that careful consideration should be placed on force field choice when modelling membrane bound proteins. These proteins frequently feature hydrophobic transmembrane segments that align with membrane thickness, which may result in membrane deformation or protein tilt when this is not the case.

We have also presented averaged lipid tail order parameters, which suggest a distinct cholesterol condensation profile for DMPC, POPC, and DOPC lipids, which is driven by cholesterol imposing different amounts of order on the same number of lipids. Averaged lipid order parameters also reveal that there is significant cholesterol condensation still occurring at high cholesterol concentrations for POPC and especially for DOPC membranes. Although this brings into question the underlying assumption of the two linear-equation model, that for high cholesterol concentrations the membrane is fully condensed and no further cholesterol condensation is observed, constraining fitting parameters suggest the exact values of the cholesterol condensing parameters reported here have little impact on the reported values of the partial-molecular areas of cholesterol.

Further work is required to better characterise the cholesterol condensation effect at higher cholesterol concentrations and in other lipid membranes. Additional experimental data would be invaluable in such further analysis. Such work will be useful to further refine and build upon the cholesterol condensation models, and allow for more accurate determination of cholesterol condensing parameters, which offer increased insight into the cholesterol condensing effect compared to solely partial-molecular areas. The analysis performed here would be particularly useful in the development and optimisation of cholesterol force fields, ensuring their accuracy in simulating biologically relevant membrane behaviour.

SUPPLEMENTARY MATERIAL

Membrane lipid content, as well as fitted parameters are provided in the supplementary material.

ACKNOWLEDGEMENTS

The authors gratefully acknowledge the use of the Iridis 5 high-performance computing facility at the University of Southampton, as well as the resources provided by the Hartree Centre (JADE2) and HECBioSim (Grant Nos. EP/R0294071/1 and EP/X035603/1) for the computational support that facilitated part of this study. This research was funded by the Engineering and Physical Sciences Research Council (EPSRC) and the Defence Science and Technology Laboratory (dstl). We would also like to express our gratitude to Sophia Wheeler for her valuable contribution through her preliminary analysis.

AUTHOR DECLARATIONS

CONFLICT OF INTEREST

This research was funded by dstl

AUTHOR CONTRIBUTIONS

Jack Sawdon: Data Curation (lead); Formal Analysis (lead); Investigation (lead); Methodology (lead); Visualisation (lead); Validation (lead); Software (lead);Writing - original draft (lead). **Thomas Piggot**: Conceptualisation (support); Data Curation (support); Validation (support); Writing - original draft (support); Supervision (support). **Jonathan Essex**: Conceptualisation (lead); Supervision (lead); Writing - review & editing (lead).

DATA AVAILABILITY STATEMENT

The data that support the findings of this study are openly available at

http://doi.org/10.5281/zenodo.13384821.

Appendix A: Single Non-linear Equation Model

Initially the partial-molecular area of cholesterol, in addition to the cholesterol condensing parameters, were calculated by fitting a single non-linear equation (eq 6)[8] to the area per lipid data across the whole range of cholesterol concentrations. The non-linear equation model was only fitted to the all-atom data, owing to fitting issues as discussed below. The resulting fits are presented in figure 7 and the corresponding parameter values are listed in the supplementary material, table S2. In addition to the simulation data presented here and the experimental data of Hung *et al.*, an additional experimental dataset from Pan *et al.*[11] is included.

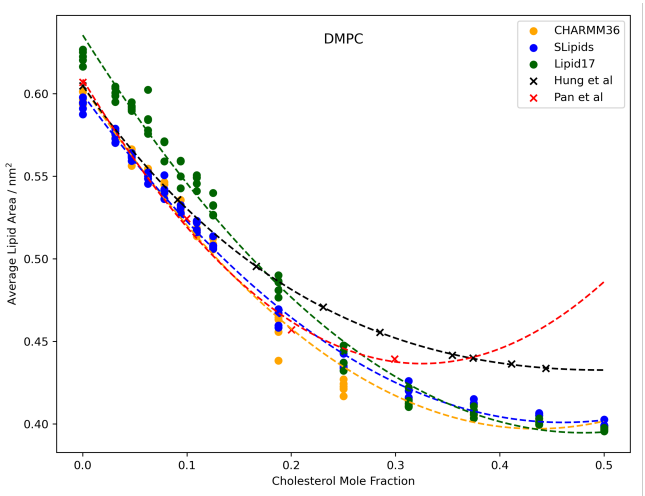

FIG. 7. Average lipid areas of all-atom force field simulations of DMPC cholesterol bilayers across a range of cholesterol concentrations (dots) were used to fit a non-linear cholesterol condensation model (dotted lines). Experimental data from Hung *et al.* and Pan *et al.* (Xs) was also used to fit the model for comparison.

It is clear from the graphical plots that the fit to the experimental data from Pan *et al.* is problematic, as observed by the prediction that the lipid area increases for cholesterol mole fractions above 0.3. For the Pan *et al.* data, the poor model behaviour is likely as a result of the data set having only 4 data points, equal to the number of parameters. We note that Pan *et al.* also fitted the single non-linear equation to their data in the original publication[11], but do not report the cholesterol condensation parameters. Pan *et al.* do report a graphical fit of the single non-linear equation, with no increase in lipid area for high cholesterol mole fractions, as opposed to the results presented here. A possible source of error in our work may be in obtaining the numerical data of Pan *et al.* from a plot in the original publication[11]. However, we believe the uncertainty added by this is less than 1%, as determined by comparison of the cholesterol mole fraction values obtained from WebPlotDigitizer and the cholesterol mole fractions used by Pan *et al.*[11]. Owing to this, such inaccuracies in extracting the data are unlikely to primarily be the cause of such large optimal parameter values. Finally, the lack of regularisation used during fitting here also likely emphasises the over-fitting, allowing the parameter norm to increase without any penalty. While regularisation is often employed in model fitting, the parameters used here have physical implications and as such, regularisation may be used to arbitrarily improve agreement with experimental data, depending on the magnitude of the penalty applied and the choice of initial parameter values.

While the remaining fits appear to be adequate from the graphical plots, there are clear fitting issues upon inspection of the fitted cholesterol condensing parameter values. Since the parameters in the models used here hold physical significance, it is not sufficient for the model to simply achieve a low error in describing the data. The values of these physical parameters must also align closely with experimental results or, in cases where ground truth data is unavailable, at least remain physically plausible.

For the simulation data, the non-linear model suggests too large values of Δa, larger than the area of a single PC lipid, and very small values of n. As Δa represents the decrease in lipid area due to condensing, it is physically impossible for this value to exceed the area of a single PC lipid; such a result implies that the area of a condensed lipid is negative. This is particularly true when fit to the Lipid17 data. While the cholesterol condensing parameters appear to be more realistic for the experimental data of Hung *et al.*, the model still predicts that each DMPC lipid is condensed by more than half of its area, and that only 2.3 neighbouring DMPC lipids are condensed, which is small considering the number of lipids which may pack around a cholesterol molecule. We suggest that the upper limit of Δa should be no more than the difference between the lipid areas of gel phase and liquid phase membranes. For example, DMPC has a gel phase lipid area of 0.47 nm^2 [80], but has an area of 0.6 nm^2 above the phase transition. Using this constraint, the upper limit of Δa for a DMPC-cholesterol bilayer is 0.13 nm^2, in good agreement with the value predicted by the two linear-equation model when fit to the Hung *et al.* dataset (table S3). Owing to these fitting issues, it was decided to adopt the two linear-equation model.

Appendix B: X-ray Form Factors

X-ray form factors were calculated from simulations and allow for a more direct comparison between simulation and experiment compared to the comparison of lipid areas, which are calculated from X-ray form factors using a set of assumptions[72,78]. We note that X-ray form factors calculated directly from simulations have system size

effects, which results in issues when defining evaluation metrics, as discussed in[81]. A metric previously defined by the NMRlipids project[81] has been employed here, and involves comparison of the first form factor minimum of experimental and simulation systems. As this method results in excluding the majority of the data by focusing on a single value of the form factor curve, we have relied more upon the comparison of lipid areas, despite this method having its own limitations.

In-house code was used to calculate X-ray form factors from simulations. While existing code exits, such as SIMtoEXP[82] and as a part of the NMRlipids databank project[81], such implementations impose limitations. SIMtoEXP employs a graphical user interface (GUI), which limits automation, while the NMRlipids databank approach, must be used in conjunction with an NMRlipids databank, imposing additional steps. The approach used here is implemented in Python, and can be used as either a command line tool, or as a Python package, allowing for flexible usage for either single simulation trajectory analysis or high throughput analysis. Our code is available at: `https://github.com/sawds/FF_MAn`.

X-ray form factors are calculated using the standard equation for lipid bilayers without assuming bilayer symmetry[81]:

$$F(q) = \left| \int_{-D/2}^{D/2} \Delta\rho_e(z) \exp izq_z dz \right| \tag{B1}$$

where $\Delta\rho_e(z)$ is the difference in total and bulk solvent electron density, z is the coordinate along the bilayer normal (assumed to be the simulation z axis) and the integral is over the simulation box of size D, centred at 0. In practice, the integral is replaced with a summation over discrete bins along the simulation z-axis (bilayer normal), with a bin width of 0.2 Å (matching the bin width used by SIMtoEXP[82]). The solvent electron density is calculated from the solvent layers above and below the bilayer. Simulation trajectories were centred on PC lipid tail termini CH_3 groups before form factors were calculated. To calculate electron density for the united-atom systems, the electron count of non-polar hydrogen atoms, which are not explicitly modelled, are added to electron count of the bonded heavy atom. Coarse-grained force fields are excluded from this analysis owing to ambiguity of electron counts of the coarse-grained beads. For example, MARTINI uses the same coarse grained topology to model DMPC and DLPC lipids, despite DLPC having two fewer carbons per acyl tail. Thus it is not obvious if the CG beads, which remain identical for both lipids, should be assigned different electron counts. Furthermore, some atoms are not assigned to a single bead in MARTINI, again complicating electron assignment. While such hurdles can be overcome, they likely require in-depth study to quantify the sensitivity of different electron assignments to the resulting X-ray form factors to be reliable. Such analysis is beyond the scope of this work.

Limited by the availability of experimental form factor data across a range of cholesterol concentrations, we compare simulations at 0 % and 30 % cholesterol mole fraction to the data of Pan et al.[11]. Unfortunately, the experimental data of Hung et al.[70] only provides X-ray intensities, and not form factors. We note that the experimental data from Pan et al. is recorded at a cholesterol mole fraction of 30 %, while the most similar simulations performed here have a cholesterol mole fraction of 31.25 %. Our analysis, following that employed by the NMRlipids project[81], focuses on the location of the first minimum of the form factor plot. The precise location of the first minimum correlates with the thickness of the membrane[81], and therefore will also correlate with membrane and lipid area. The main advantage of this approach, as opposed to metrics based on residuals between experimental and simulation data, is that the precise locations of form factor minima are invariant to simulation box size and does not require scaling of the simulation form factors to match the relative intensity scale of experiments. While robust simulation corrections have been proposed to address the impact of system size on relative lobe heights[83], these corrections were not implemented in the NMRLipids study[81], and hence were not adopted here. Thus while this method allows for a simple and more direct comparison between simulation and experimental data, it also reduces the (already limited) amount of experimental data available for comparison.

The Cartesian distances between experimental and simulation form factor first minimum locations are presented in figure 8. Experimental values taken from[11] were extracted from graphical plots using WebPlotDigitizer[71].

The comparison of experimental form factor data to simulation offers a more mixed result compared to the area data. Generally force fields more closely align with experiment for pure PC membranes compared to PC cholesterol membranes mixtures. All-atom force fields consistently under predict the minimum location, while united-atom forcefields over-predict in DMPC and under-predict in DOPC. The form factor analysis here does not show the same correlation of our previous analysis, which suggests that all-atom force fields better model cholesterol containing DMPC lipid systems. Indeed, for the lipid area analysis, CHARMM36 was one of the best performing force fields, however diverges the most from experimental form factor minimum locations. This may be due to the over-reliance on only two cholesterol concentrations per lipid, compounded by using only a single point from the from factor curves. The critical lack of more experimental data is of particular concern when performing this analysis, due to it necessitating excluding most of the form factor curve.

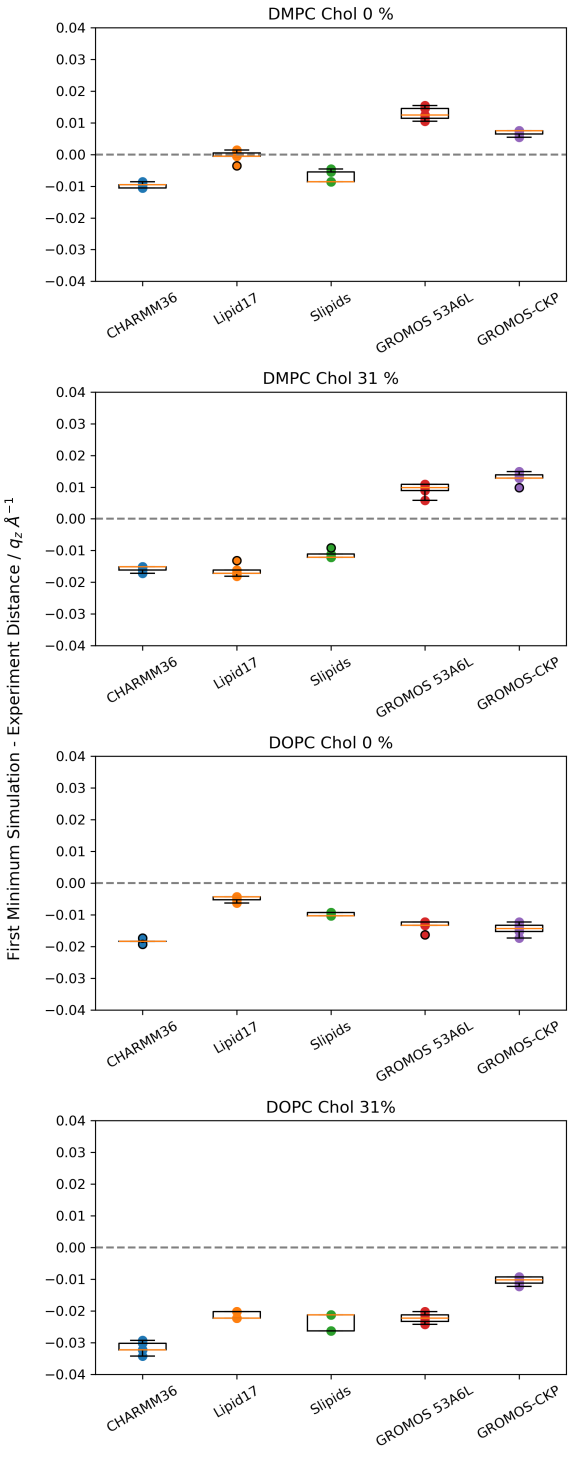

FIG. 8. Cartesian distances between the location of the first minima in X-ray form factors of experimental and simulation systems. Each data point represents an independent replica. Experimental data was recorded at 0 % and 30 % cholesterol mole fractions.

[1] D. Casares, P. V. Escribá, and C. A. Rosselló, International Journal of Molecular Sciences **20**, 2167 (2019).
[2] K. Komatsuya, N. Kikuchi, T. Hirabayashi, and K. Kasahara, International Journal of Molecular Sciences **24**, 5566 (2023).
[3] M. Bogdanov, Emerg Top Life Sci **7**, 1 (2023).
[4] S. Sonnino and A. Prinetti, Current Medicinal Chemistry **20**, 4 (2013).
[5] G. van Meer, D. R. Voelker, and G. W. Feigenson, Nat Rev Mol Cell Biol **9**, 112 (2008).
[6] P. Shamaprasad, C. O. Frame, T. C. Moore, A. Yang, C. R. Iacovella, J. A. Bouwstra, A. L. Bunge, and C. McCabe, Progress in lipid research , 101184 (2022).
[7] T. L. Steck and Y. Lange, Traffic **19**, 750 (2018).
[8] O. Edholm and J. F. Nagle, Biophysical Journal **89**, 1827 (2005).
[9] Y. Su, Q. Li, L. Chen, and Z. Yu, Colloids and Surfaces A: Physicochemical and Engineering Aspects **293**, 123 (2007).
[10] M. Kodama, O. Shibata, S. Nakamura, S. Lee, and G. Sugihara, Colloids and Surfaces B: Biointerfaces **33**, 211 (2004).
[11] J. Pan, S. Tristram-Nagle, and J. F. Nagle, Physical Review E - Statistical, Nonlinear, and Soft Matter Physics **80**, 1 (2009).
[12] A. Zampelas and E. Magriplis, Nutrients **11**, 1645 (2019).
[13] S. L. Regen, JACS Au **2**, 84 (2022).
[14] J. B. Leathes, The Lancet **205**, 853 (1925).
[15] P. Dynarowicz-Łatka and K. Hac-Wydro, Colloids and Surfaces B: Biointerfaces **37**, 21 (2004).
[16] M. R. Krause, M. Wang, L. Mydock-McGrane, D. F. Covey, E. Tejada, P. F. Almeida, and S. L. Regen, Langmuir **30**, 12114 (2014).
[17] M. L. Berkowitz, Biochimica et Biophysica Acta (BBA) - Biomembranes **1788**, 86 (2009).
[18] Y. Wang, P. Gkeka, J. E. Fuchs, K. R. Liedl, and Z. Cournia, Biochimica et Biophysica Acta (BBA) - Biomembranes **1858**, 2846 (2016).
[19] Q. Waheed, R. Tjörnhammar, and O. Edholm, Biophysical Journal **103**, 2125 (2012).
[20] S. Chiu, E. Jakobsson, R. J. Mashl, and H. L. Scott, Biophysical Journal **83**, 1842 (2002).
[21] M. D. Daily, B. N. Olsen, P. H. Schlesinger, D. S. Ory, and N. A. Baker, Journal of Chemical Theory and Computation **10**, 2137 (2014).
[22] P. Siani, H. Khandelia, M. Orsi, and L. G. Dias, Journal of Computer-Aided Molecular Design **32**, 1259 (2018).
[23] M. Alwarawrah, J. Dai, and J. Huang, The Journal of Physical Chemistry B **114**, 7516 (2010).
[24] C. L. Armstrong, D. Marquardt, H. Dies, N. Kučerka, Z. Yamani, T. A. Harroun, J. Katsaras, A. C. Shi, and M. C. Rheinstädter, PLoS ONE **8** (2013).
[25] F. Leeb and L. Maibaum, Biophysical Journal **115**, 2179 (2018).
[26] F. De Meyer and B. Smit, Proceedings of the National Academy of Sciences of the United States of America **106**, 3654 (2009).
[27] S. Wheeler, *Physical properties of mixed membranes explored using atomistic and coarse grained molecular dynamic simulations with enhanced sampling techniques*, Ph.D. thesis, University of Southampton, School of Chemistry (2018).
[28] S. Seo and W. Shinoda, Journal of Chemical Theory and Computation **15**, 762 (2019).
[29] A. K. Smith and D. K. Klimov, Journal of Physical Chemistry B **122**, 11311 (2018).
[30] S. Baoukina, E. Mendez-Villuendas, W. F. Bennett, and D. P. Tieleman, Faraday Discussions **161**, 63 (2012).
[31] H. Martinez-Seara, T. Róg, M. Karttunen, I. Vattulainen, and R. Reigada, PLoS ONE **5**, e11162 (2010).
[32] Z. Cournia, G. M. Ullmann, and J. C. Smith, The Journal of Physical Chemistry B **111**, 1786 (2007).
[33] M. I. Oh, C. I. Oh, and D. F. Weaver, Journal of Physical Chemistry B **124**, 3686 (2020).
[34] F. Fornasier, L. M. P. de Souza, F. R. de Souza, F. Reynaud, and A. S. Pimentel, Journal of Chemical Information and Modeling , acs.jcim.9b00830 (2020).
[35] I. Ermilova and A. P. Lyubartsev, Soft Matter **15**, 78 (2019).

[36]M. Javanainen, P. Heftberger, J. J. Madsen, M. S. Miettinen, G. Pabst, and O. H. S. Ollila, J. Chem. Theory Comput. **19**, 6342 (2023).
[37]J. B. Klauda, R. M. Venable, J. A. Freites, J. W. O'Connor, D. J. Tobias, C. Mondragon-Ramirez, I. Vorobyov, A. D. MacKerell, and R. W. Pastor, Journal of Physical Chemistry B **114**, 7830 (2010).
[38]F. Grote and A. P. Lyubartsev, The journal of physical chemistry. B **124**, 8784 (2020).
[39]I. Gould, A. Skjevik, C. Dickson, B. Madej, and R. Walker, Manuscript in preparation (2018).
[40]C. J. Dickson, B. D. Madej, A. Skjevik, R. M. Betz, K. Teigen, I. R. Gould, and R. C. Walker, Journal of Chemical Theory and Computation **10**, 865 (2014).
[41]B. D. Madej, I. R. Gould, and R. C. Walker, The Journal of Physical Chemistry B **119**, 12424 (2015).
[42]D. Poger, W. F. Van Gunsteren, and A. E. Mark, Journal of Computational Chemistry **31**, 1117 (2010).
[43]T. J. Piggot, A. Piñeiro, and S. Khalid, J. Chem. Theory Comput. **8**, 4593 (2012).
[44]S. J. Marrink, A. H. De Vries, T. A. Harroun, J. Katsaras, and S. R. Wassall, Journal of the American Chemical Society **130**, 10 (2008).
[45]M. N. Melo, H. I. Ingólfsson, and S. J. Marrink, Journal of Chemical Physics **143**, 243152 (2015).
[46]L. Borges-Araújo, A. C. Borges-Araújo, T. N. Ozturk, D. P. Ramirez-Echemendia, B. Fábián, T. S. Carpenter, S. Thallmair, J. Barnoud, H. I. Ingólfsson, G. Hummer, D. P. Tieleman, S. J. Marrink, P. C. T. Souza, and M. N. Melo, J. Chem. Theory Comput. **19**, 7387 (2023).
[47]P. C. T. Souza, R. Alessandri, J. Barnoud, S. Thallmair, I. Faustino, F. Grünewald, I. Patmanidis, H. Abdizadeh, B. M. H. Bruininks, T. A. Wassenaar, P. C. Kroon, J. Melcr, V. Nieto, V. Corradi, H. M. Khan, J. Domański, M. Javanainen, H. Martinez-Seara, N. Reuter, R. B. Best, I. Vattulainen, L. Monticelli, X. Periole, D. P. Tieleman, A. H. De Vries, and S. J. Marrink, Nat Methods **18**, 382 (2021).
[48]S. Genheden and J. W. Essex, J Comput Aided Mol Des **30**, 969 (2016).
[49]A. K. Malde, L. Zuo, M. Breeze, M. Stroet, D. Poger, P. C. Nair, C. Oostenbrink, and A. E. Mark, J. Chem. Theory Comput. **7**, 4026 (2011).
[50]M. Stroet, B. Caron, M. S. Engler, J. van der Woning, A. Kauffmann, M. van Dijk, M. El-Kebir, K. M. Visscher, J. Holownia, C. Macfarlane, B. J. Bennion, S. Gelpi-Dominguez, F. C. Lightstone, T. van der Storm, D. P. Geerke, A. E. Mark, and G. W. Klau, J Comput Aided Mol Des **37**, 357 (2023).
[51]M. Bachar, P. Brunelle, D. P. Tieleman, and A. Rauk, J. Phys. Chem. B **108**, 7170 (2004).
[52]A. Kukol, J. Chem. Theory Comput. **5**, 615 (2009).
[53]T. Piggot, J. Essex, and J. Allison, Manuscipt in preparation (2024).
[54]L. Martinez, R. Andrade, E. G. Birgin, and J. M. Martínez, Journal of Computational Chemistry **30**, 2157 (2009).
[55]J. Nagle, R. Zhang, S. Tristram-Nagle, W. Sun, H. Petrache, and R. Suter, Biophysical Journal **70**, 1419 (1996).
[56]R. J. Mashl, H. L. Scott, S. Subramaniam, and E. Jakobsson, Biophysical Journal **81**, 3005 (2001).
[57]K. Hristova and S. H. White, Biophysical Journal **74**, 2419 (1998).
[58]M. J. Abraham, T. Murtola, R. Schulz, S. Páll, J. C. Smith, B. Hess, and E. Lindah, SoftwareX **1-2**, 19 (2015).
[59]A. P. Thompson, H. M. Aktulga, R. Berger, D. S. Bolintineanu, W. M. Brown, P. S. Crozier, P. J. in 't Veld, A. Kohlmeyer, S. G. Moore, T. D. Nguyen, R. Shan, M. J. Stevens, J. Tranchida, C. Trott, and S. J. Plimpton, Computer Physics Communications **271**, 108171 (2022).
[60]H. J. Berendsen, J. P. Postma, W. F. Van Gunsteren, A. Dinola, and J. R. Haak, The Journal of Chemical Physics **81**, 3684 (1984).
[61]S. Genheden and J. W. Essex, J. Chem. Theory Comput. **11**, 4749 (2015).
[62]M. Tuckerman, B. J. Berne, and G. J. Martyna, The Journal of Chemical Physics **97**, 1990 (1992).
[63]D. J. Evans and B. L. Holian, The Journal of Chemical Physics **83**, 4069 (1985).
[64]G. Bussi, D. Donadio, and M. Parrinello, The Journal of Chemical Physics **126**, 014101 (2007).
[65]P.-C. Hsu, B. M. H. Bruininks, D. Jefferies, P. C. T. de Souza, J. Lee, D. S. Patel, S. J. Marrink, Y. Qi, S. Khalid, and W. Im, Journal of computational chemistry **38**, 2354 (2017).
[66]M. Parrinello and A. Rahman, Journal of Applied Physics **52**, 7182 (1981).
[67]T. N. Heinz, W. F. van Gunsteren, and P. H. Hünenberger, The Journal of Chemical Physics **115**, 1125 (2001).
[68]S. Thallmair, M. Javanainen, B. Fábián, H. Martinez-Seara, and S. J. Marrink, The Journal of Physical Chemistry B **125**, 9537 (2021).
[69]K. W. Vugrin, L. P. Swiler, R. M. Roberts, N. J. Stucky-Mack, and S. P. Sullivan, Water Resources Research **43** (2007).
[70]W. C. Hung, M. T. Lee, F. Y. Chen, and H. W. Huang, Biophysical Journal **92**, 3960 (2007).
[71]A. Rohatgi, "WebPlotDigitizer," (2024).
[72]N. Kučerka, J. F. Nagle, J. N. Sachs, S. E. Feller, J. Pencer, A. Jackson, and J. Katsaras, Biophysical Journal **95**, 2356 (2008).
[73]Y. Liu and J. F. Nagle, Physical Review E - Statistical Physics, Plasmas, Fluids, and Related Interdisciplinary Topics **69**, 4 (2004).
[74]H. M. McConnell and A. Radhakrishnan, Biochimica et Biophysica Acta (BBA) - Biomembranes **1610**, 159 (2003).
[75]T. H. Chou and C. H. Chang, Colloids and Surfaces B: Biointerfaces **17**, 71 (2000).
[76]T. Róg, M. Pasenkiewicz-Gierula, I. Vattulainen, and M. Karttunen, Biochimica et Biophysica Acta (BBA) - Biomembranes **1788**, 97 (2009).
[77]T. M. Ferreira, F. Coreta-Gomes, O. H. Samuli Ollila, M. J. Moreno, W. L. Vaz, and D. Topgaard, Physical Chemistry Chemical Physics **15**, 1976 (2013).
[78]M. C. Wiener and S. H. White, Biophysical Journal **61**, 434 (1992).
[79]C. Wang, M. R. Krause, and S. L. Regen, Journal of the American Chemical Society **137**, 664 (2015).
[80]S. Tristram-Nagle, Y. Liu, J. Legleiter, and J. F. Nagle, Biophysical Journal **83**, 3324 (2002).
[81]A. M. Kiirikki, H. S. Antila, L. S. Bort, P. Buslaev, F. Favela-Rosales, T. M. Ferreira, P. F. J. Fuchs, R. Garcia-Fandino, I. Gushchin, B. Kav, N. Kučerka, P. Kula, M. Kurki, A. Kuzmin, A. Lalitha, F. Lolicato, J. J. Madsen, M. S. Miettinen, C. Mingham, L. Monticelli, R. Nencini, A. M. Nesterenko, T. J. Piggot, Á. Piñeiro, N. Reuter, S. Samantray, F. Suárez-Lestón, R. Talandashti, and O. H. S. Ollila, Nature Communications **15**, 1136 (2024).
[82]N. Kučerka, J. Katsaras, and J. F. Nagle, The Journal of membrane biology **235**, 43 (2010).
[83]A. R. Braun, E. G. Brandt, O. Edholm, J. F. Nagle, and J. N. Sachs, Biophysical Journal **100**, 2112 (2011).